



**U.S. ARMY RESEARCH,
DEVELOPMENT AND
ENGINEERING COMMAND**

**TITLE: Design and Experimental Results for the S415
Airfoil**

AUTHOR: Dan M. Somers and Mark D. Maughmer

COMPANY NAME: Airfoils, Incorporated

**COMPANY ADDRESS: 122 Rose Drive
Port Matilda PA 16870-7535**

DATE: August 2010

**FINAL REPORT: Contract Number W911W6-07-C-0047, SBIR Phase II,
Topic Number A06-006, Proposal Number A2-2972**

DISTRIBUTION STATEMENT A

Approved for public release; distribution is unlimited.

Prepared for:

**U.S. ARMY RESEARCH, DEVELOPMENT AND ENGINEERING COMMAND,
AVIATION APPLIED TECHNOLOGY DIRECTORATE, FORT EUSTIS, VA 23604-5577**

AIRFOILS, INCORPORATED

122 ROSE DRIVE

PORT MATILDA, PA 16870-7535 USA

WEBSITE WWW.AIRFOILS.COM

TELEPHONE (814) 357-0500

FACSIMILE (814) 357-0357

**DESIGN AND EXPERIMENTAL
RESULTS FOR THE S415 AIRFOIL**

DAN M. SOMERS

AIRFOILS, INCORPORATED

MARK D. MAUGHMER

THE PENNSYLVANIA STATE UNIVERSITY

AUGUST 2010

ABSTRACT

A 14.12-percent-thick, natural-laminar-flow airfoil, the S415, intended for the rotor of a helicopter in hover has been designed and analyzed theoretically and verified experimentally in The Pennsylvania State University Low-Speed, Low-Turbulence Wind Tunnel. The two primary objectives of high maximum lift and low profile drag have been achieved. The constraint on the pitching moment has been satisfied. The airfoil exhibits a docile stall. Comparisons of the theoretical and experimental results generally show good agreement.

INTRODUCTION

Almost all airfoils in use on rotorcraft today were developed under the assumption that extensive laminar flow is not likely on a rotor. (See ref. 1, for example.) For the present application, however, given the moderate Reynolds numbers and the exploratory nature of the current effort, the achievement of laminar flow warrants examination.

The airfoil designed under the present effort is intended for the rotor of a helicopter in hover. The airfoil would then be morphed into a shape more suitable for cruise. (See ref. 2.) To complement the design effort, an investigation was conducted in The Pennsylvania State University Low-Speed, Low-Turbulence Wind Tunnel (ref. 3) to obtain the basic, low-speed, two-dimensional aerodynamic characteristics of the airfoil. The results have been compared with predictions from the method of references 4 and 5 and from the method of reference 6.

SYMBOLS

Values are given in both SI and U.S. Customary Units. Measurements and calculations were made in U.S. Customary Units.

C_p pressure coefficient, $\frac{P_l - P_\infty}{q_\infty}$

c airfoil chord, mm (in.)

c_c section chord-force coefficient, $\oint C_p d\left(\frac{z}{c}\right)$

c_d section profile-drag coefficient, $\int_{\text{Wake}} c_d' d\left(\frac{h}{c}\right)$, except post stall,
 $c_n \sin \alpha + c_c \cos \alpha$

c_d' point drag coefficient (ref. 7)

c_l section lift coefficient, $c_n / \cos \alpha - c_d \tan \alpha$

c_m	section pitching-moment coefficient about quarter-chord point, $-\oint C_p \left(\frac{x}{c} - 0.25 \right) d \left(\frac{x}{c} \right) + \oint C_p \left(\frac{z}{c} \right) d \left(\frac{z}{c} \right)$
c_n	section normal-force coefficient, $-\oint C_p d \left(\frac{x}{c} \right)$
h	horizontal width in wake profile, mm (in.)
M	free-stream Mach number
p	static pressure, Pa (lbf/ft ²)
q	dynamic pressure, Pa (lbf/ft ²)
R	Reynolds number based on free-stream conditions and airfoil chord
s	arc length along airfoil surface, mm (in.)
t	airfoil thickness, mm (in.)
x	airfoil abscissa, mm (in.)
y	model span station, $y = 0$ at midspan, mm (in.)
z	airfoil ordinate, mm (in.)
α	angle of attack relative to x-axis, deg

Subscripts:

l	local point on airfoil
ll	lower limit of low-drag range
max	maximum
min	minimum
S	separation
T	transition
ul	upper limit of low-drag range

∞ free-stream conditions

Abbreviations:

L. lower surface

NACA National Advisory Committee for Aeronautics

S. boundary-layer separation location, x_S/c

T. boundary-layer transition location, x_T/c

U. upper surface

AIRFOIL DESIGN

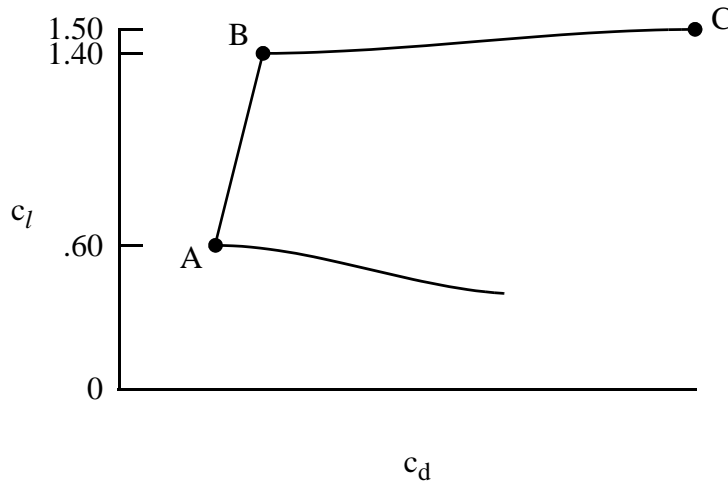
OBJECTIVES AND CONSTRAINTS

The airfoil design specifications are contained in table I. Two primary objectives are evident. The first objective is to achieve a maximum lift coefficient of 1.50 at a Mach number of 0.50 and a Reynolds number of 5.00×10^6 . A requirement related to this objective is that the maximum lift coefficient not decrease significantly with transition fixed near the leading edge on both surfaces. In addition, the airfoil should exhibit docile stall characteristics at a Mach number of 0.2 and a Reynolds number of 2.0×10^6 , which is within the operational range of the Penn State Low-Speed, Low-Turbulence Wind Tunnel. The second objective is to obtain low profile-drag coefficients from a lift coefficient of 0.60 to 1.40 at a Mach number of 0.50 and a Reynolds number of 5.00×10^6 .

One major constraint was placed on the design of the airfoil. At a Mach number of 0.40 and a Reynolds number of 4.00×10^6 , the pitching-moment coefficient at a lift coefficient of 1.5 must be no more negative than -0.10 .

PHILOSOPHY

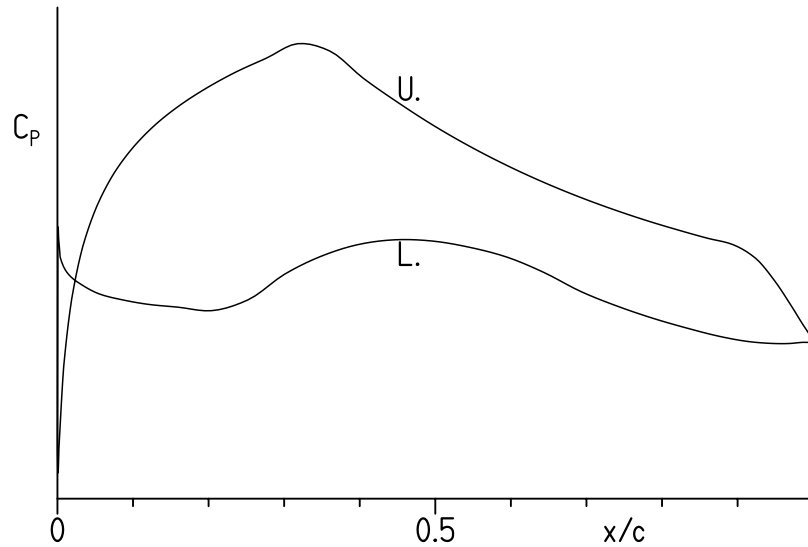
Given the above objectives and constraint, certain characteristics of the design are apparent. The following sketch illustrates a drag polar that meets the goals for this design.



Sketch 1

The desired airfoil shape can be traced to the pressure distributions that occur at the various points in sketch 1. Point A is the lower limit of the low-drag range of lift coefficients; point B, the upper limit. The profile-drag coefficient at point B is not as low as at point A, unlike the polars of many laminar-flow airfoils where the drag coefficient within the laminar bucket is nearly constant. (See, for example, ref. 8.) This characteristic is related to the elimination of significant (i.e., drag-producing) laminar separation bubbles on the upper surface for the design range of Reynolds numbers. (See ref. 9.) The drag coefficient increases rapidly outside the low-drag, lift-coefficient range because boundary-layer transition moves quickly toward the leading edge with increasing (or decreasing) lift coefficient. This feature results in a leading-edge shape that produces a suction peak at higher lift coefficients, which ensures that transition on the upper surface will occur very near the leading edge. Thus, the maximum lift coefficient, point C, occurs with turbulent flow along the entire upper surface and, therefore, should be relatively insensitive to roughness at the leading edge.

From the preceding discussion, the pressure distributions along the polar can be deduced. The pressure distribution at point A should look something like sketch 2.



Sketch 2

To achieve low drag, a favorable pressure gradient is desirable along the upper surface to about 30-percent chord. Aft of this point, a short region having a shallow, adverse pressure gradient (i.e., a “transition ramp”) promotes the efficient transition from laminar to turbulent flow (ref. 10). The transition ramp is followed by a concave pressure recovery, which exhibits lower drag and has less tendency to separate than the corresponding linear or convex pressure recovery (ref. 10). The specific pressure recovery employed represents a compromise between maximum lift, drag, pitching moment, stall characteristics, and drag divergence. The steep, adverse pressure gradient aft of about 90-percent chord is a “separation ramp,” originally proposed by F. X. Wortmann,¹ which confines turbulent separation to a small region near the trailing edge. By constraining the movement of the separation point at high angles of attack, higher lift coefficients can be achieved with little drag penalty. (See ref. 11.) This feature has the added benefit of promoting docile stall characteristics. (See ref. 12.)

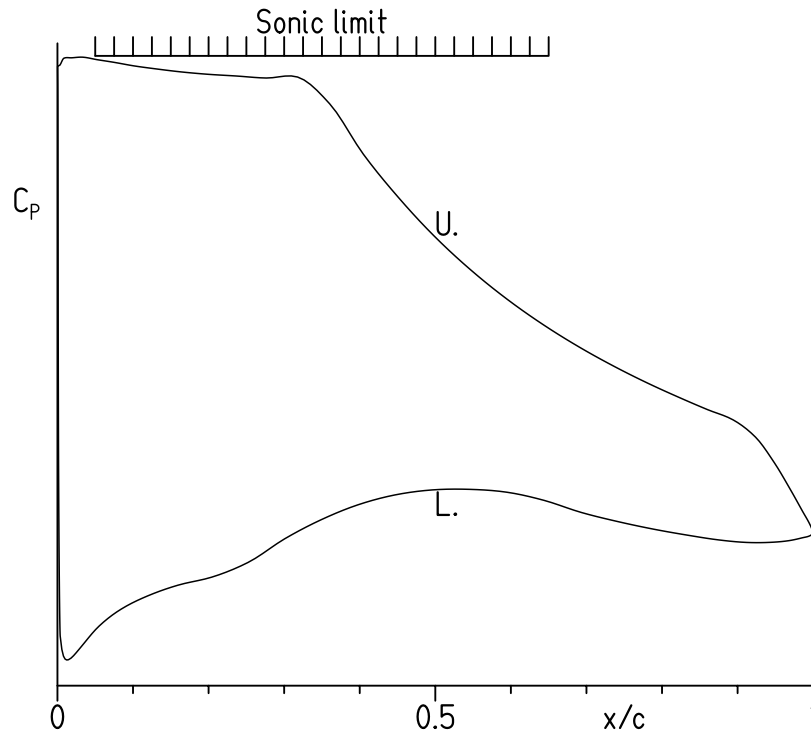
Along the lower surface, the pressure gradient is initially adverse and then favorable to about 45-percent chord. Thus, transition is imminent over the forward portion of the lower surface. (See ref. 13.) This concept allows a wide low-drag range to be achieved and increases the loading in the leading-edge region. The forward loading serves to balance, with respect to the pitching-moment constraint, the aft loading, both of which contribute to the

¹Director, Institute for Aerodynamics and Gas Dynamics, University of Stuttgart, Germany, 1974–1985.

achievement of a high maximum lift coefficient and low profile-drag coefficients. This region is followed by a transition ramp and then a concave pressure recovery.

The amounts of pressure recovery on the upper and lower surfaces are determined by the width of the low-drag, lift-coefficient range and the pitching-moment constraint.

At point B, the pressure distribution should look like sketch 3.



Sketch 3

No suction peak exists at the leading edge. Instead, a moderately adverse pressure gradient extends from the leading edge to the beginning of the pressure recovery.

EXECUTION

Given the pressure distributions previously discussed, the design of the airfoil is reduced to the inverse problem of transforming the pressure distributions into an airfoil shape. The Eppler Airfoil Design and Analysis Code (refs. 4 and 5) was used because of its unique capability for multipoint design and because of confidence gained during the design, analysis, and experimental verification of many other airfoils. (See ref. 14, for example.)

The airfoil is designated the S415. The airfoil shape and coordinates are available from Airfoils, Incorporated. The airfoil thickness is 14.12-percent chord.

THEORETICAL PROCEDURE

The theoretical results are predicted using the method of references 4 and 5 (PROFIL07), commonly known as the Eppler code, and the method of reference 6 (MSES 3.0). Critical amplification factors of 11 and 9 were specified for the boundary-layer transition computations using the method of references 4 and 5 and the method of reference 6, respectively. Because the maximum lift coefficient computed by the method of references 4 and 5 is not always realistic, an empirical criterion has been applied to the computed results. The criterion assumes the maximum lift coefficient has been reached if the drag coefficient of the upper surface reaches a certain value that is a function of the Reynolds number and the wind-tunnel facility. It should also be noted that the compressibility correction (ref. 15) incorporated in the method of references 4 and 5 is invalid if the local flow is supersonic.

Because the free-stream Mach number for all wind-tunnel test conditions did not exceed 0.2, the flow can be considered essentially incompressible for the purpose of comparing the theoretical and experimental results. This allows the (incompressible) conformal-mapping (design) method of references 4 and 5 and the fast, subcritical flow solver of the method of reference 6 to be used.

EXPERIMENTAL PROCEDURE

WIND TUNNEL

The Pennsylvania State University Low-Speed, Low-Turbulence Wind Tunnel (ref. 3) is a closed-throat, single-return, atmospheric tunnel (fig. 1). The test section is 101.3 cm (39.9 in.) high by 147.6 cm (58.1 in.) wide (fig. 2). Electrically actuated turntables provide positioning and attachment for the two-dimensional model. The turntables are flush with the top and bottom tunnel walls and rotate with the model. The axis of rotation coincided approximately with midchord. The model was mounted vertically between the turntables and the gaps between the model and the turntables were sealed. The turbulence intensity in the test section is approximately 0.05 percent at 46 m/s (150 ft/s).

MODEL

The aluminum, wind-tunnel model was fabricated by Advanced Technologies, Incorporated, Newport News, Virginia, using a numerically controlled milling machine. The model had a chord of 533.38 mm (20.999 in.) and a span of 107.95 cm (42.50 in.) and, thus, extended through both turntables. Upper- and lower-surface orifices were located to one side of mid-span at the staggered positions listed in table II. All the orifices were 0.51 mm (0.020 in.) in diameter with their axes perpendicular to the surface. The surfaces of the model were sanded

to ensure an aerodynamically smooth finish. The measured model contour was within 0.13 mm (0.005 in.) of the prescribed shape.

WAKE-SURVEY PROBE

A total- and static-pressure, wake-survey probe (fig. 3) was mounted from the top tunnel wall (fig. 2). The probe was positioned 50.8 cm (20.0 in.) from the ceiling (i.e., about midspan) and automatically aligned with the wake-centerline streamline. A traverse mechanism incrementally positioned the probe to survey the wake. The increment was 1.27 mm (0.050 in.) for traverses less than 254.0 mm (10.00 in.) and 2.54 mm (0.100 in.) for longer traverses, which were occasionally required near the maximum lift coefficient. The tip of the probe was located 0.6 chord downstream of the trailing edge of the model.

INSTRUMENTATION

Basic tunnel pressures and the wake pressures were measured with precision transducers. Measurements of the pressures on the model were made by an automatic pressure-scanning system utilizing precision transducers. Data were obtained and recorded by an electronic data-acquisition system.

METHODS

The pressures measured on the model were reduced to standard pressure coefficients and numerically integrated to obtain section normal-force and chord-force coefficients and section pitching-moment coefficients about the quarter-chord point. Section profile-drag coefficients were computed from the wake total and static pressures by the method of reference 7. Wake surveys were not performed, however, at most post-stall angles of attack, in which case, the profile-drag coefficients were computed from the normal- and chord-force coefficients.

Standard, low-speed, wind-tunnel boundary corrections (ref. 16) have been applied to the data. It should be noted that the model-chord-to-tunnel-height ratio is 0.36, which is approaching the limit of 0.4 given in reference 16. The wake-survey-probe total-pressure-tube displacement correction (ref. 7) has been taken into account.

TESTS

The model was tested at Reynolds numbers based on airfoil chord of 1.0×10^6 , 1.5×10^6 , and 2.0×10^6 with transition free (smooth) and with transition fixed by roughness near the leading edge, 2-percent chord on the upper surface and 5-percent chord on the lower surface, to simulate full-chord, turbulent flow. The grit roughness was sized using the method of reference 17 and sparsely distributed along 3-mm (0.1-in.) wide strips applied to the model

with lacquer. (See table III(a).) The model was also tested with a roughness equivalent to NACA standard roughness (ref. 8), which consisted of grit roughness having a nominal size of 0.249 mm (0.0098 in.) applied to the model with lacquer and sparsely distributed from the leading edge to an arc length of 8-percent chord on the upper and lower surfaces. (See table III(b).) (The grit size was scaled from the NACA standard-roughness grit size by the ratio of the model chords used in the two wind tunnels: 533.4 mm (21.00 in.) in the present investigation and 609.6 mm (24.00 in.) in the NACA tests.)

The Mach number did not exceed 0.2 for any test condition. Thus, the test Mach numbers and Reynolds numbers are much lower than the operational values of the intended application.

Starting from 1° , which is within the low-drag range of lift coefficients, the angle of attack was decreased to near that for zero lift. The angle of attack was then increased from 1° to post-stall values.

DISCUSSION OF RESULTS

THEORETICAL RESULTS

Pressure Distributions

The pressure distributions predicted using the method of reference 6 (MSES 3.0) at various angles of attack at a Mach number of 0.50 and a Reynolds number of 5.00×10^6 are shown in figure 4.

Section Characteristics

The section characteristics predicted using the method of references 4 and 5 (PROFIL07) and the method of reference 6 (MSES 3.0) at a Mach number of 0.50 and a Reynolds number of 5.00×10^6 with transition free and with transition fixed are shown in figure 5. (It should be remembered that the compressibility correction incorporated in the method of refs. 4 and 5 is invalid if the local flow is supersonic and, accordingly, only subsonic results are shown.) Based on the predictions, all the design objectives and the design constraint have essentially been met.

EXPERIMENTAL RESULTS

Pressure Distributions

The pressure distributions at various angles of attack for a Reynolds number of 1.5×10^6 and a Mach number of 0.1 with transition free are shown in figure 6. At an angle of attack of -5.10° (fig. 6(a)), a short laminar separation bubble is discernible on the upper sur-

face around 55-percent chord and a long laminar separation bubble is evident on the lower surface aft of the leading edge. As the angle of attack is increased, the short bubble on the upper surface moves forward and the long bubble on the lower surface decreases in length, until it has disappeared at an angle of attack of -2.02° (fig. 6(a)). At an angle of attack of 0.03° (fig. 6(b)), a short laminar separation bubble is evident on the lower surface around 65-percent chord, the laminar flow having survived the pressure peak near the leading edge. As the angle of attack is increased further, the bubble on the upper surface continues to move forward, whereas the bubble on the lower surface migrates slowly aft (figs. 6(b)–6(d)). At an angle of attack of 8.23° (fig. 6(d)), turbulent, trailing-edge separation is evident on the upper surface. The amount of separation increases with increasing angle of attack (fig. 6(d)). The maximum lift coefficient occurs at an angle of attack just beyond 9.24° (fig. 6(d)). As the angle of attack is increased even further, the separation point continues to move forward and the leading-edge peak continues to climb (fig. 6(e)).

Section Characteristics

The section characteristics with transition free, with transition fixed, and with scaled, NACA standard roughness, denoted “rough,” are shown in figure 7 and tabulated in the appendix. For a Reynolds number of 2.0×10^6 and a Mach number of 0.2 with transition free (fig. 7(c)), the maximum lift coefficient is 1.37 and the stall characteristics are relatively docile. The lower limit of the low-drag, lift-coefficient range is 0.50; the upper limit, 1.28. For a Reynolds number of 1.5×10^6 and a Mach number of 0.1 with transition free (fig. 7(b)), the zero-lift pitching-moment coefficient is -0.09 .

The effects of Reynolds number on the section characteristics are summarized in figure 8. In general, the lift-curve slope, the maximum lift coefficient, the lower limit of the low-drag range, and the magnitude of the pitching-moment coefficients increase with increasing Reynolds number and the stall characteristics become less docile. The profile-drag coefficients and the upper limit of the low-drag range decrease with increasing Reynolds number.

The effect of fixing transition on the section characteristics is shown in figure 7. In general, the lift-curve slope, the maximum lift coefficient, and the magnitude of the pitching-moment coefficients decrease with transition fixed. These results are primarily a consequence of the boundary-layer displacement effect, which decambers the airfoil because the displacement thickness is greater with transition fixed than with transition free. In addition, the maximum lift coefficient decreases with transition fixed because the roughness induces earlier trailing-edge separation. The reduction in maximum lift coefficient averages 4 percent over the test Reynolds number range. The drag coefficients are, of course, adversely affected by the roughness.

It should be noted that, for many test conditions, the Reynolds number based on local velocity and boundary-layer displacement thickness at the roughness locations is too low to support turbulent flow. (See ref. 18.) Accordingly, to force transition, the roughness must be so large that it increases the displacement thickness, which abnormally decreases the lift coefficient and the magnitude of the pitching-moment coefficient and increases the drag coeffi-

cient. Conversely, at low lift coefficients, the roughness on the upper surface, which is sized for high lift coefficients, is too small to force transition, resulting in incorrectly low drag coefficients.

The effect of the scaled, NACA standard roughness on the section characteristics is shown in figure 7. The effect is more severe than that of fixing transition. The reduction in maximum lift coefficient is larger, averaging 13 percent over the test Reynolds number range. It should be remembered that the effect of roughness is proportional to the ratio of the roughness height to the boundary-layer thickness. Because the height of the scaled, NACA standard roughness and the airfoil chord are constant, the effect of this roughness typically increases with increasing Reynolds number (because increasing Reynolds number results in decreasing boundary-layer thickness), although the effect on the maximum lift coefficient is almost constant over the test Reynolds number range.

The variations of maximum lift coefficient and minimum profile-drag coefficient with Reynolds number are shown in figures 9 and 10, respectively. In general, the maximum lift coefficient increases with increasing Reynolds number, whereas the minimum profile-drag coefficient decreases, which are typical trends for most airfoils.

COMPARISON OF THEORETICAL AND EXPERIMENTAL RESULTS

Pressure Distributions

The comparison of the theoretical and experimental pressure distributions at various angles of attack is shown in figure 11. It should be noted that the pressure distributions predicted using the method of references 4 and 5 (PROFIL07) are inviscid and incompressible, whereas the pressure distributions predicted using the method of reference 6 (MSES 3.0) as well as the experimental pressure distributions were obtained for a Reynolds number of 1.5×10^6 and a Mach number of 0.1 with transition free. It should also be noted that the theoretical lift coefficient from the method of references 4 and 5 is calculated from the lift-curve slope and the angle of attack relative to the zero-lift line, whereas the lift coefficient from the method of reference 6 and from the experiment is derived from the integrated pressure distribution. (See refs. 4–7.) Thus, at a given lift coefficient, the pressure distribution predicted using the method of references 4 and 5 does not necessarily have the same area as the measured pressure distribution.

With respect to the method of references 4 and 5, at lift coefficients of 0.48 and 0.93 (figs. 11(a) and 11(b), respectively), the pressure coefficients and the pressure gradients agree reasonably well, except in the vicinity of the laminar separation bubbles and near the trailing edge. The latter disparity is probably the result of the boundary-layer displacement effect. At a lift coefficient of 1.33 (fig. 11(c)), which is just below the measured maximum lift coefficient, the agreement is poor because the effect of the upper-surface, trailing-edge separation on the pressure distribution is not modelled in the method of references 4 and 5.

With respect to the method of reference 6, at a lift coefficient of 0.48 (fig. 11(a)), the pressure coefficients and the pressure gradients agree reasonably well, except near the trailing edge on the upper surface. The location of the upper-surface laminar separation bubble is predicted well, but that of the lower-surface bubble is forward of the measured location. At a lift coefficient of 0.93 (fig. 11(b)), the pressure distributions again agree reasonably well, and the locations of the bubbles are predicted well. At a lift coefficient of 1.33 (fig. 11(c)), the agreement is poor because the significant, upper-surface, trailing-edge separation is not predicted by the method of reference 6.

Section Characteristics

The comparison of the theoretical and experimental section characteristics with transition free is shown in figure 12. The maximum lift coefficient is estimated within approximately 1 percent using the empirical criterion previously discussed applied to the results from the method of references 4 and 5 (PROFIL07). The method of reference 6 (MSES 3.0) overpredicts the maximum lift coefficient by an average of 13 percent. The method of reference 6 underpredicts the profile-drag coefficients. The method of references 4 and 5 underpredicts and the method of reference 6 overpredicts the upper limit of the low-drag, lift-coefficient range. The method of references 4 and 5 overpredicts the magnitude of the pitching-moment coefficients.

The comparison of the theoretical and experimental section characteristics with transition fixed is shown in figure 13. In general, the predicted characteristics show similar tendencies as with transition free, although the general agreement is poorer, probably because of the abnormalities introduced by the roughness, as discussed previously. In particular, the method of reference 6 overpredicts the maximum lift coefficient by an average of 18 percent.

CONCLUDING REMARKS

A 14.12-percent-thick, natural-laminar-flow airfoil, the S415, intended for the rotor of a helicopter in hover has been designed and analyzed theoretically and verified experimentally in The Pennsylvania State University Low-Speed, Low-Turbulence Wind Tunnel. The two primary objectives of a high maximum lift coefficient and low profile-drag coefficients have been achieved. The constraint on the pitching-moment coefficient has been satisfied. The airfoil exhibits docile stall characteristics. Comparisons of the theoretical and experimental results generally show good agreement.

ACKNOWLEDGMENTS

This effort was sponsored by the U.S. Army. Preston B. Martin served as the technical monitor.

REFERENCES

1. Noonan, Kevin W.: Aerodynamic Characteristics of Two Rotorcraft Airfoils Designed for Application to the Inboard Region of a Main Rotor Blade. NASA TP-3009, 1990.
2. Kota, Sridhar; Ervin, Gregory; Osborn, Russell; and Ormiston, Robert A.: Design and Fabrication of an Adaptive Leading Edge Rotor Blade. American Helicopter Soc. 64th Annual Forum, Montreal, Canada, April 29 – May 1, 2008.
3. Brophy, Christopher M.: Turbulence Management and Flow Qualification of The Pennsylvania State University Low Turbulence, Low Speed, Closed Circuit Wind Tunnel. M. S. Thesis, Pennsylvania State Univ., 1993.
4. Eppler, Richard: Airfoil Design and Data. Springer-Verlag (Berlin), 1990.
5. Eppler, Richard: Airfoil Program System “PROFIL07.” User’s Guide. Richard Eppler, c.2007.
6. Drela, M.: Design and Optimization Method for Multi-Element Airfoils. AIAA Paper 93-0969, Feb. 1993.
7. Pankhurst, R. C.; and Holder, D. W.: Wind-Tunnel Technique. Sir Isaac Pitman & Sons, Ltd. (London), 1965.
8. Abbott, Ira H.; Von Doenhoff, Albert E.; and Stivers, Louis S., Jr.: Summary of Airfoil Data. NACA Rep. 824, 1945. (Supersedes NACA WR L-560.)
9. Eppler, Richard; and Somers, Dan M.: Airfoil Design for Reynolds Numbers Between 50,000 and 500,000. Proceedings of the Conference on Low Reynolds Number Airfoil Aerodynamics, UNDAS-CP-77B123, Univ. of Notre Dame, June 1985, pp. 1–14.
10. Wortmann, F. X.: Experimental Investigations on New Laminar Profiles for Gliders and Helicopters. TIL/T.4906, British Minist. Aviat., Mar. 1960. (Translated from Z. Flugwissenschaften, Bd. 5, Heft 8, Aug. 1957, S. 228–243.)
11. Eppler, R.: Comparison of Theoretical and Experimental Profile Drags. NASA TT F-16981, 1976. (Translated from Schweizer Aero-Revue, vol. 38, no. 10, Oct. 1963, pp. 593–595.)
12. Maughmer, Mark D.; and Somers, Dan M.: Design and Experimental Results for a High-Altitude, Long-Endurance Airfoil. J. Aircr., vol. 26, no. 2, Feb. 1989, pp. 148–153.
13. Eppler, R.: Laminar Airfoils for Reynolds Numbers Greater Than 4×10^6 . B-819-35, Apr. 1969. (Available from NTIS as N69-28178; translated from Ingenieur-Archiv, Bd. 38, Heft 4/5, 1969, S. 232–240.)

14. Somers, Dan M.: Subsonic Natural-Laminar-Flow Airfoils. *Natural Laminar Flow and Laminar Flow Control*, R. W. Barnwell and M. Y. Hussaini, eds., Springer-Verlag New York, Inc., 1992, pp. 143–176.
15. Labrujere, Th. E.; Loeve, W.; and Sloof, J. W.: An Approximate Method for the Determination of the Pressure Distribution on Wings in the Lower Critical Speed Range. *Transonic Aerodynamics*. AGARD CP No. 35, Sept. 1968, pp. 17-1–17-10.
16. Allen, H. Julian; and Vincenti, Walter G.: Wall Interference in a Two-Dimensional-Flow Wind Tunnel, With Consideration of the Effect of Compressibility. NACA Rep. 782, 1944. (Supersedes NACA WR A-63.)
17. Braslow, Albert L.; and Knox, Eugene C.: Simplified Method for Determination of Critical Height of Distributed Roughness Particles for Boundary-Layer Transition at Mach Numbers From 0 to 5. NACA TN 4363, 1958.
18. Schubauer, G. B.; and Klebanoff, P. S.: Contributions on the Mechanics of Boundary-Layer Transition. NACA Rep. 1289, 1956.

TABLE I.- AIRFOIL DESIGN SPECIFICATIONS

Parameter	Objective/ Constraint	Mach Number M	Reynolds Number R	Priority
Minimum lift coefficient $c_{l,min}$	0.40	0.50	5.00×10^6	Medium
Maximum lift coefficient $c_{l,max}$	1.50			High
Lower limit of low-drag, lift-coefficient range $c_{l,ll}$	0.60			Medium
Upper limit of low-drag, lift-coefficient range $c_{l,ul}$	1.40			High
Pitching-moment coefficient c_m at $c_l = 1.5$	≥ -0.10	0.40	4.00×10^6	Low
Thickness t/c	—			—
Other: Maximum lift coefficient $c_{l,max}$ relatively independent of leading-edge roughness Docile stall characteristics at $M = 0.2$ and $R = 2.0 \times 10^6$ (i.e., verifiable in tunnel)				

TABLE II.- MODEL ORIFICE LOCATIONS

[c = 533.38 mm (20.999 in.)]

Upper Surface		Lower Surface	
x/c	y, mm (in.)	x/c	y, mm (in.)
0.00160	-129.31 (-5.091)	0.00000	-149.16 (-5.873)
.00814	-128.44 (-5.057)	.00319	-148.14 (-5.832)
.01876	-127.47 (-5.019)	.01408	-146.87 (-5.782)
.03339	-125.86 (-4.955)	.03185	-145.14 (-5.714)
.05237	-124.29 (-4.893)	.05515	-142.86 (-5.624)
.07463	-121.78 (-4.795)	.08426	-140.01 (-5.512)
.10121	-119.35 (-4.699)	.11951	-136.88 (-5.389)
.13064	-116.40 (-4.582)	.15934	-132.87 (-5.231)
.16370	-112.93 (-4.446)	.20402	-128.43 (-5.056)
.19875	-109.47 (-4.310)	.25191	-123.96 (-4.880)
.23670	-106.06 (-4.176)	.30051	-119.28 (-4.696)
.27655	-102.26 (-4.026)	.34825	-115.02 (-4.528)
.31781	-98.07 (-3.861)	.39710	-109.98 (-4.330)
.36033	-94.12 (-3.705)	.44586	-105.13 (-4.139)
.40492	-89.77 (-3.534)	.49582	-100.36 (-3.951)
.45107	-85.05 (-3.349)	.54463	-95.54 (-3.761)
.49838	-80.48 (-3.169)	.59492	-90.52 (-3.564)
.54661	-76.02 (-2.993)	.64423	-85.74 (-3.376)
.59565	-78.60 (-3.094)	.69319	-81.02 (-3.190)
.64354	-81.49 (-3.208)	.74148	-76.15 (-2.998)
.69157	-84.54 (-3.328)	.78943	-80.98 (-3.188)
.73792	-87.24 (-3.435)	.83365	-85.50 (-3.366)
.78196	-89.99 (-3.543)	.87502	-89.92 (-3.540)
.82338	-92.42 (-3.638)	.91162	-93.86 (-3.695)
.86120	-94.59 (-3.724)	.94305	-97.11 (-3.823)
.89419	-96.19 (-3.787)	.96748	-99.59 (-3.921)
.92556	-98.30 (-3.870)	.98520	-101.35 (-3.990)
.95187	-99.90 (-3.933)	.99667	-103.88 (-4.090)
.97271	-101.13 (-3.981)		
.98764	-101.81 (-4.008)		
.99748	-102.30 (-4.027)		
1.00000	-96.63 (-3.804)		

TABLE III.- ROUGHNESS LOCATIONS AND SIZES

(a) Transition Fixed

R	Upper surface			Lower surface		
	x/c	Grit number	Nominal size, mm (in.)	x/c	Grit number	Nominal size, mm (in.)
1.0×10^6	0.02	90	0.178 (0.0070)	0.05	46	0.419 (0.0165)
1.5×10^6		100	0.150 (0.0059)		60	0.297 (0.0117)
2.0×10^6		150	0.104 (0.0041)		70	0.249 (0.0098)

(b) Scaled, NACA Standard Roughness

R	Upper surface			Lower surface		
	s/c	Grit number	Nominal size, mm (in.)	s/c	Grit number	Nominal size, mm (in.)
1.0×10^6	0 to 0.08	70	0.249 (0.0098)	0 to 0.08	70	0.249 (0.0098)
1.5×10^6						
2.0×10^6						

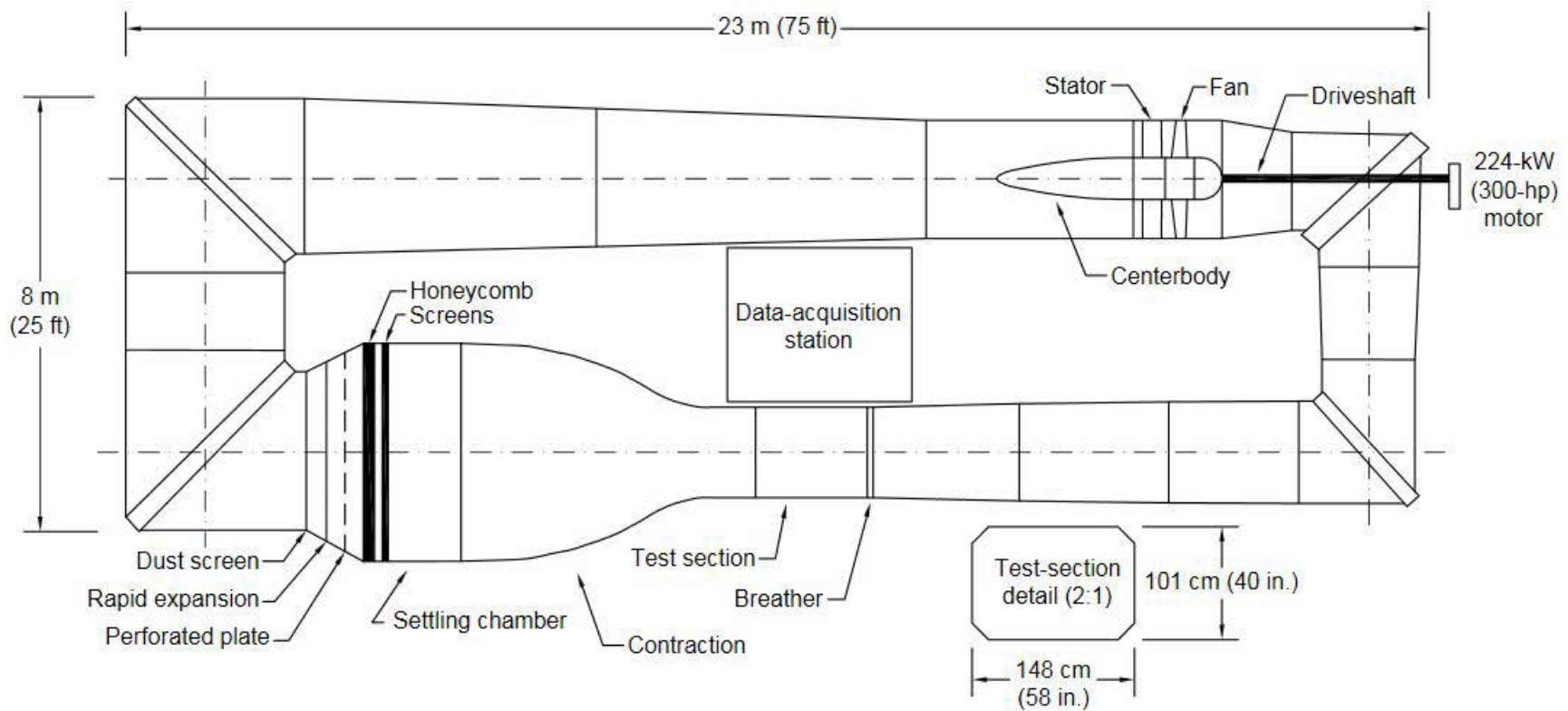


Figure 1.- The Pennsylvania State University Low-Speed, Low-Turbulence Wind Tunnel.



Figure 2.- S415 airfoil model and wake-survey probe mounted in test section.

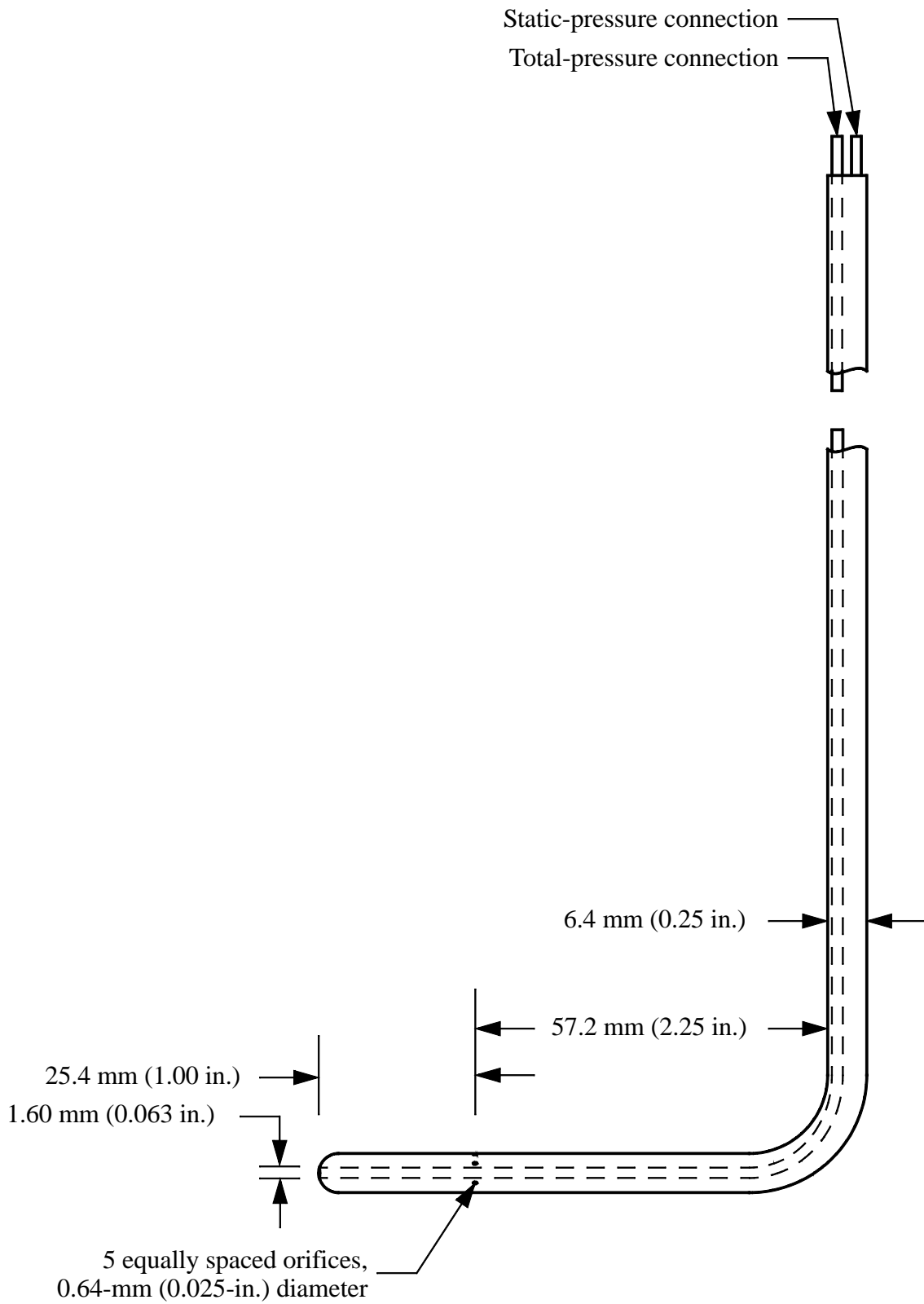
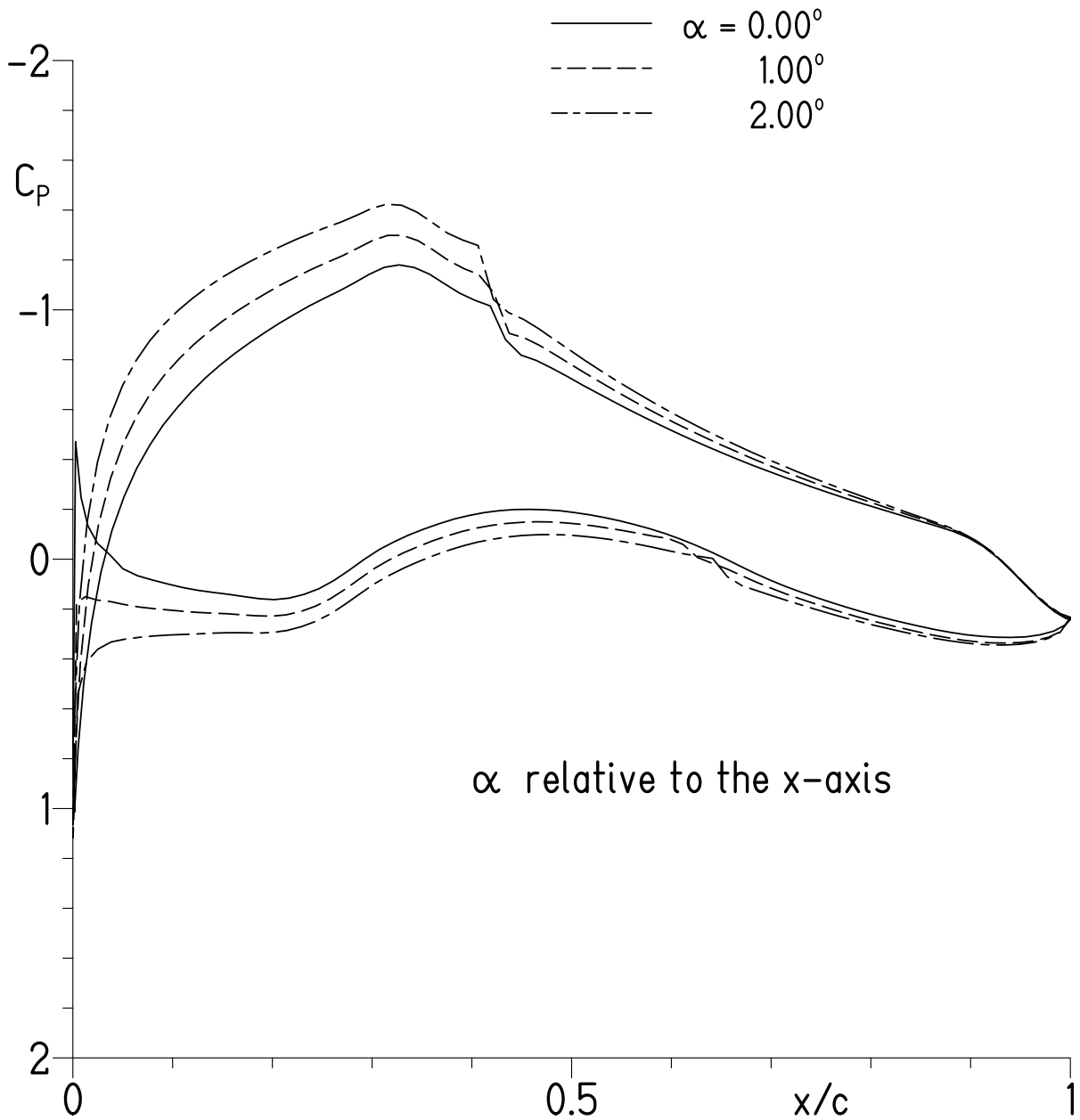
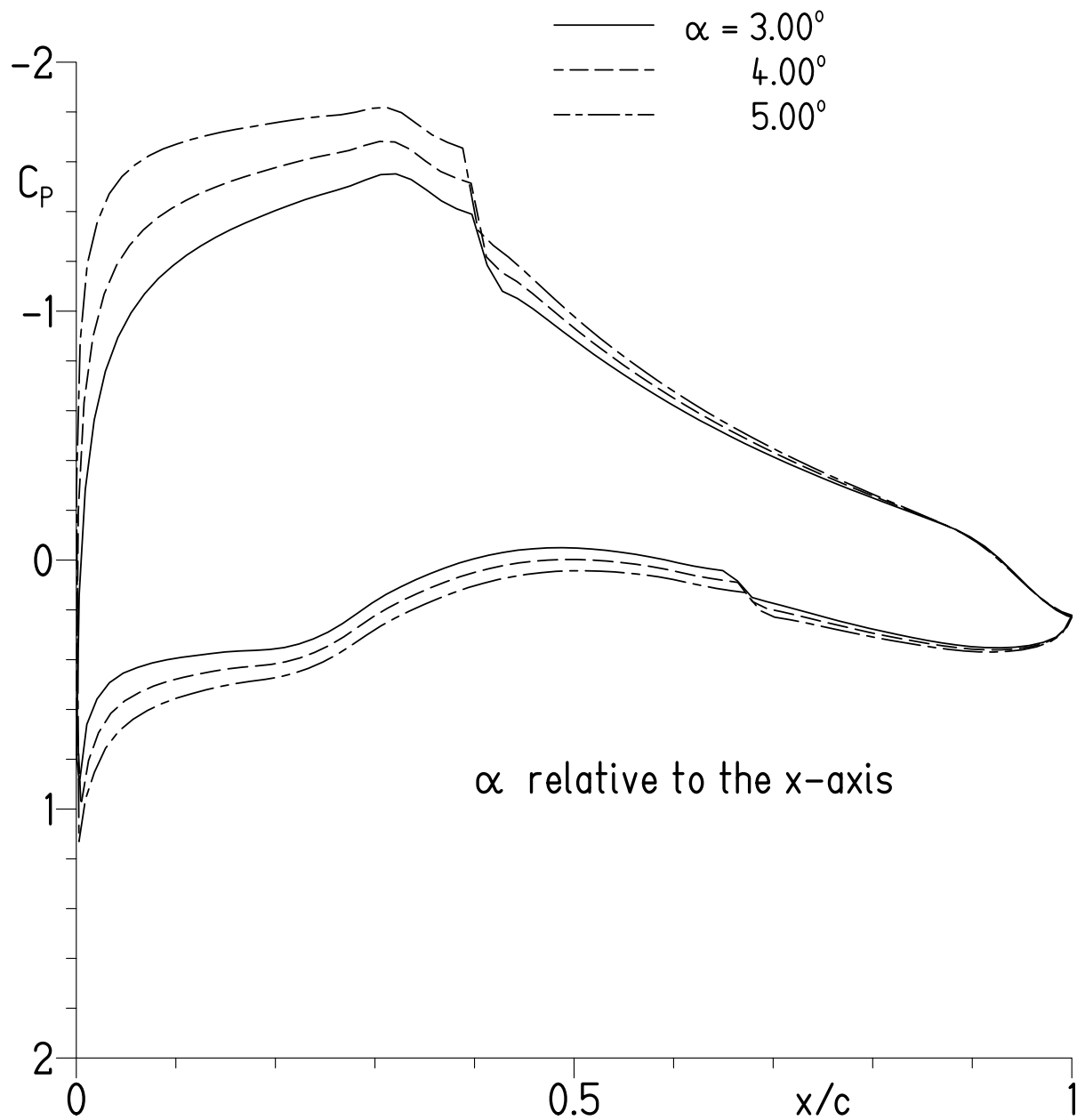


Figure 3.- Wake-survey probe.



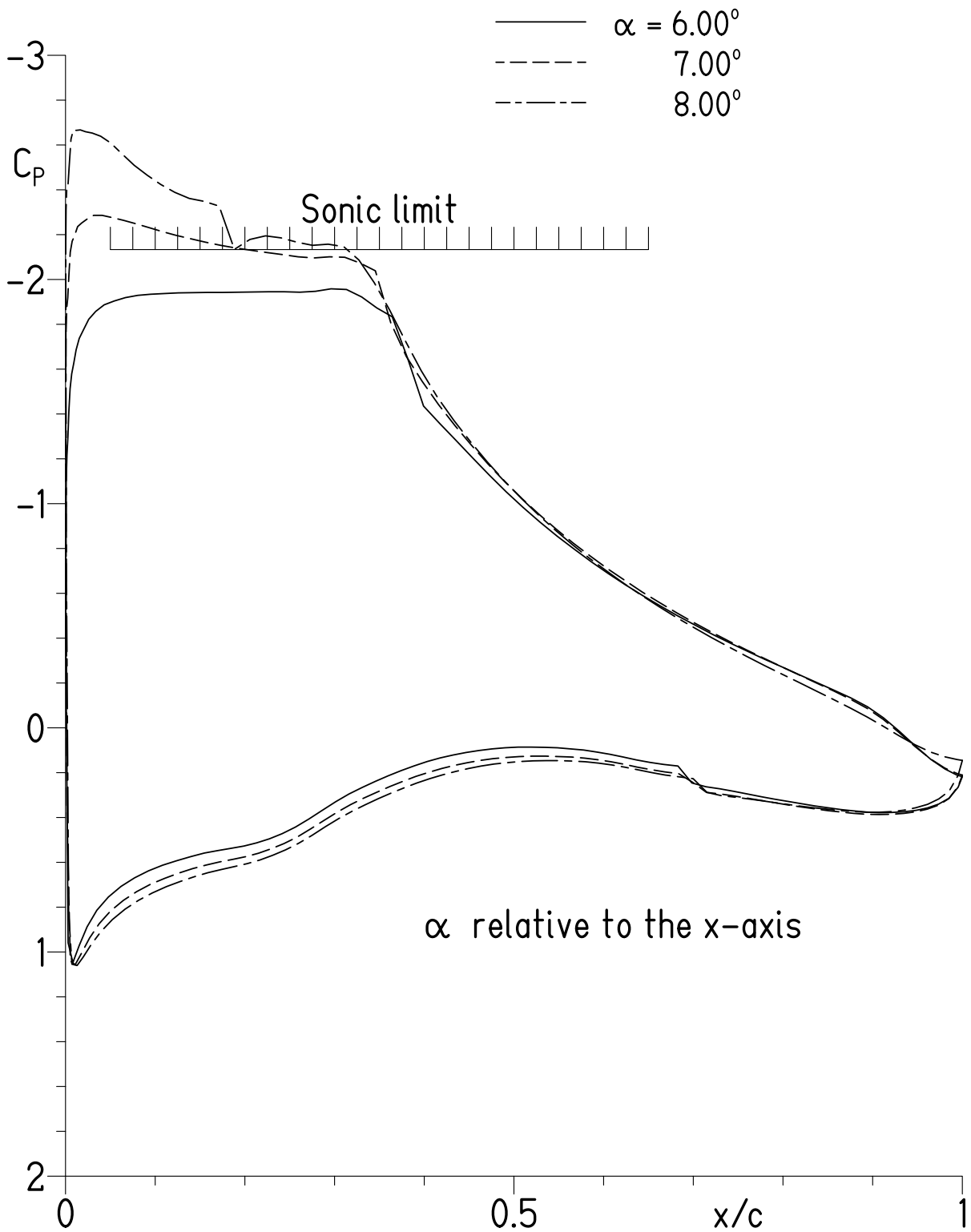
(a) $\alpha = 0.00^\circ, 1.00^\circ, \text{ and } 2.00^\circ$.

Figure 4.- Theoretical pressure distributions at $M = 0.50$ and $R = 5.00 \times 10^6$.



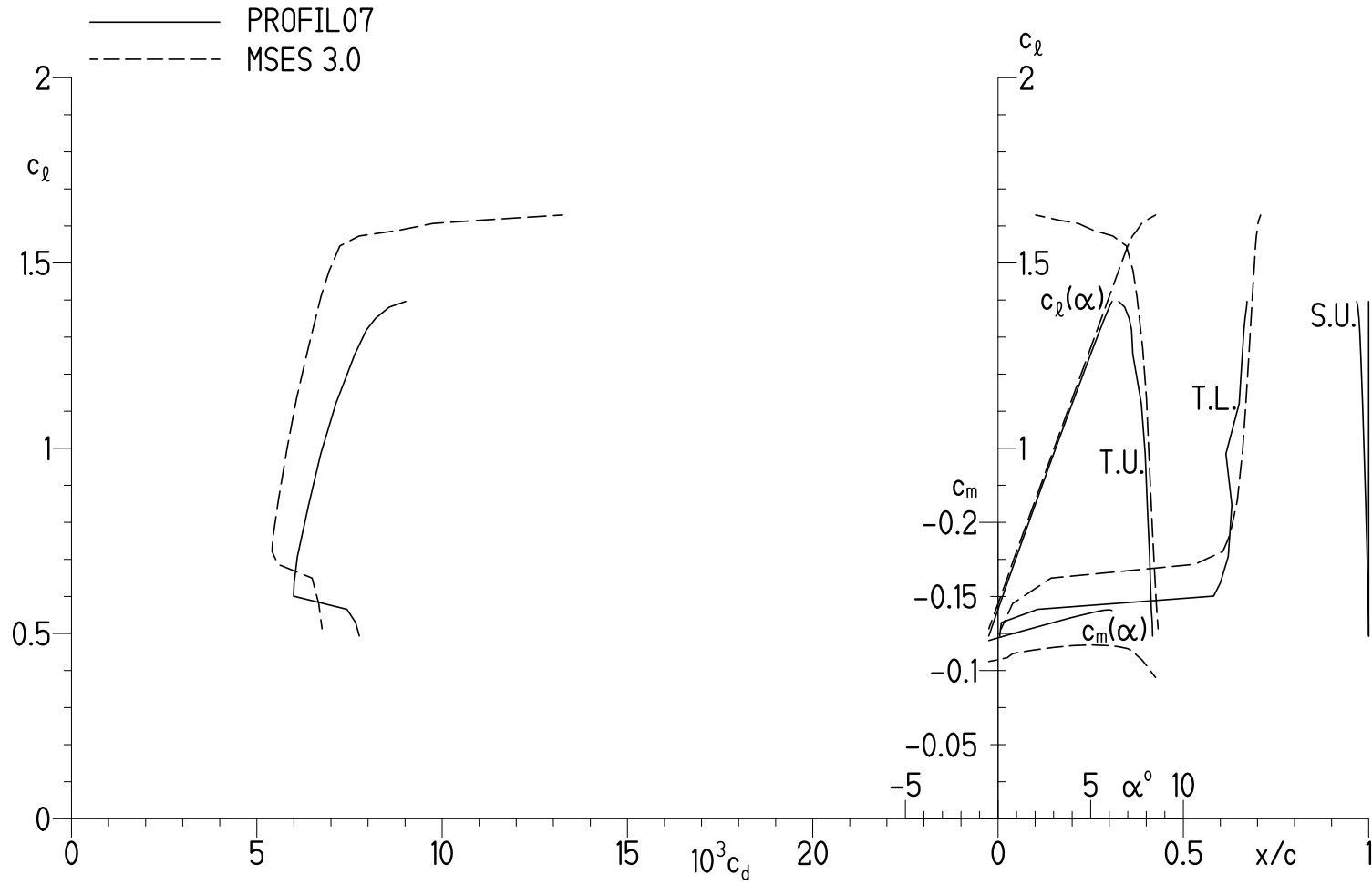
(b) $\alpha = 3.00^\circ, 4.00^\circ,$ and 5.00° .

Figure 4.- Continued.



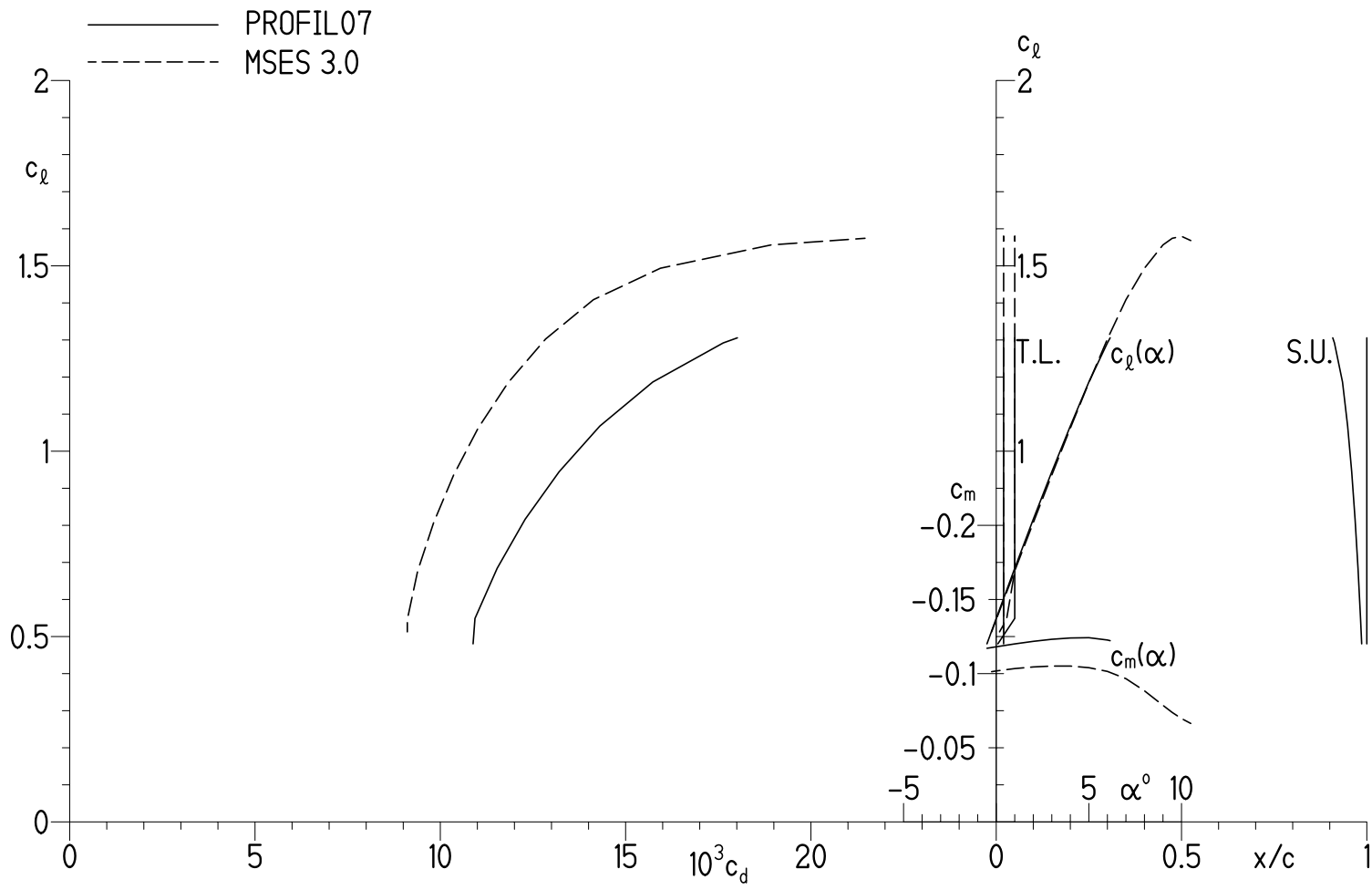
(c) $\alpha = 6.00^\circ, 7.00^\circ, \text{ and } 8.00^\circ$.

Figure 4.- Concluded.



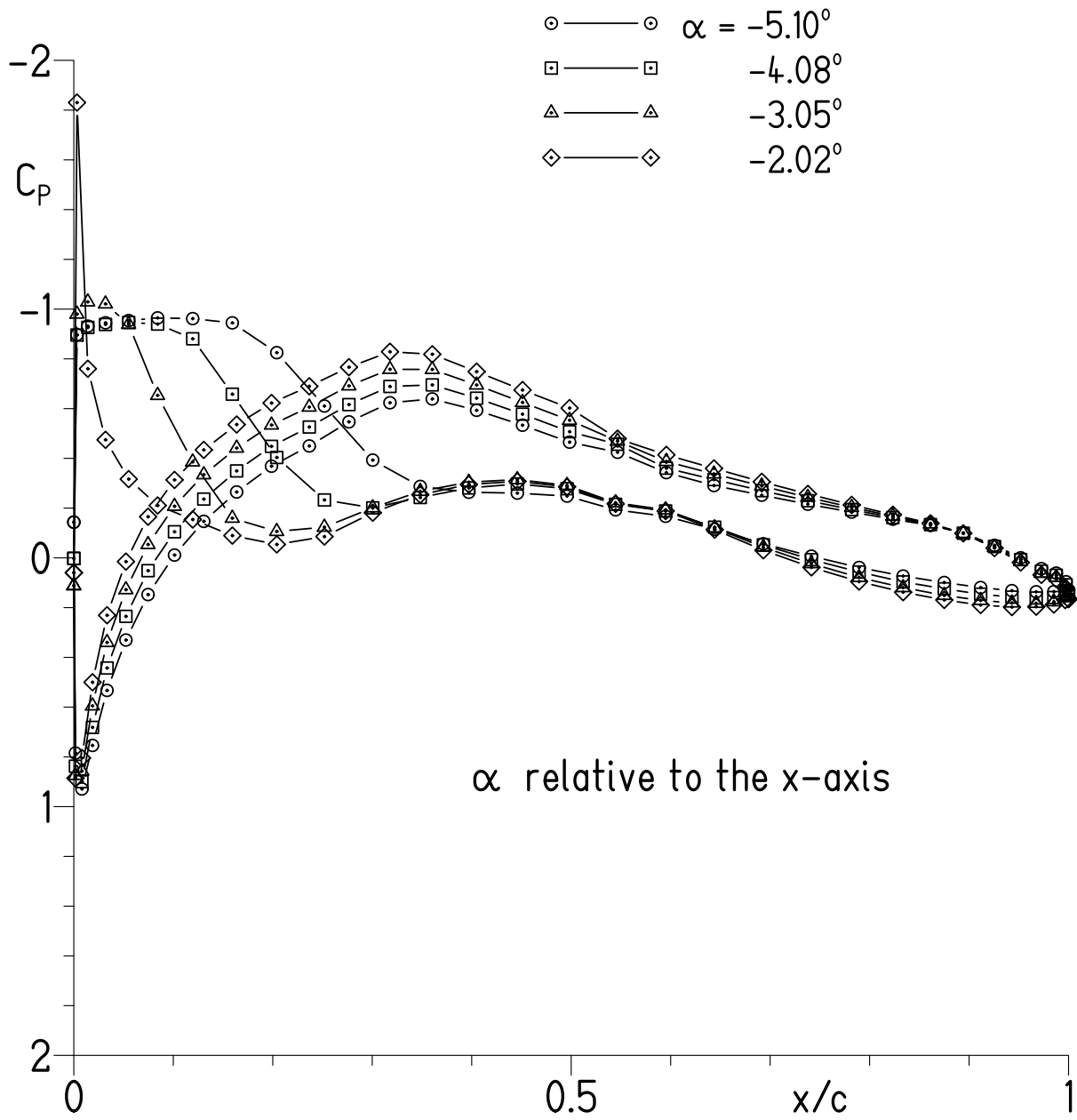
(a) Transition free.

Figure 5.- Theoretical section characteristics at $M = 0.50$ and $R = 5.00 \times 10^6$.



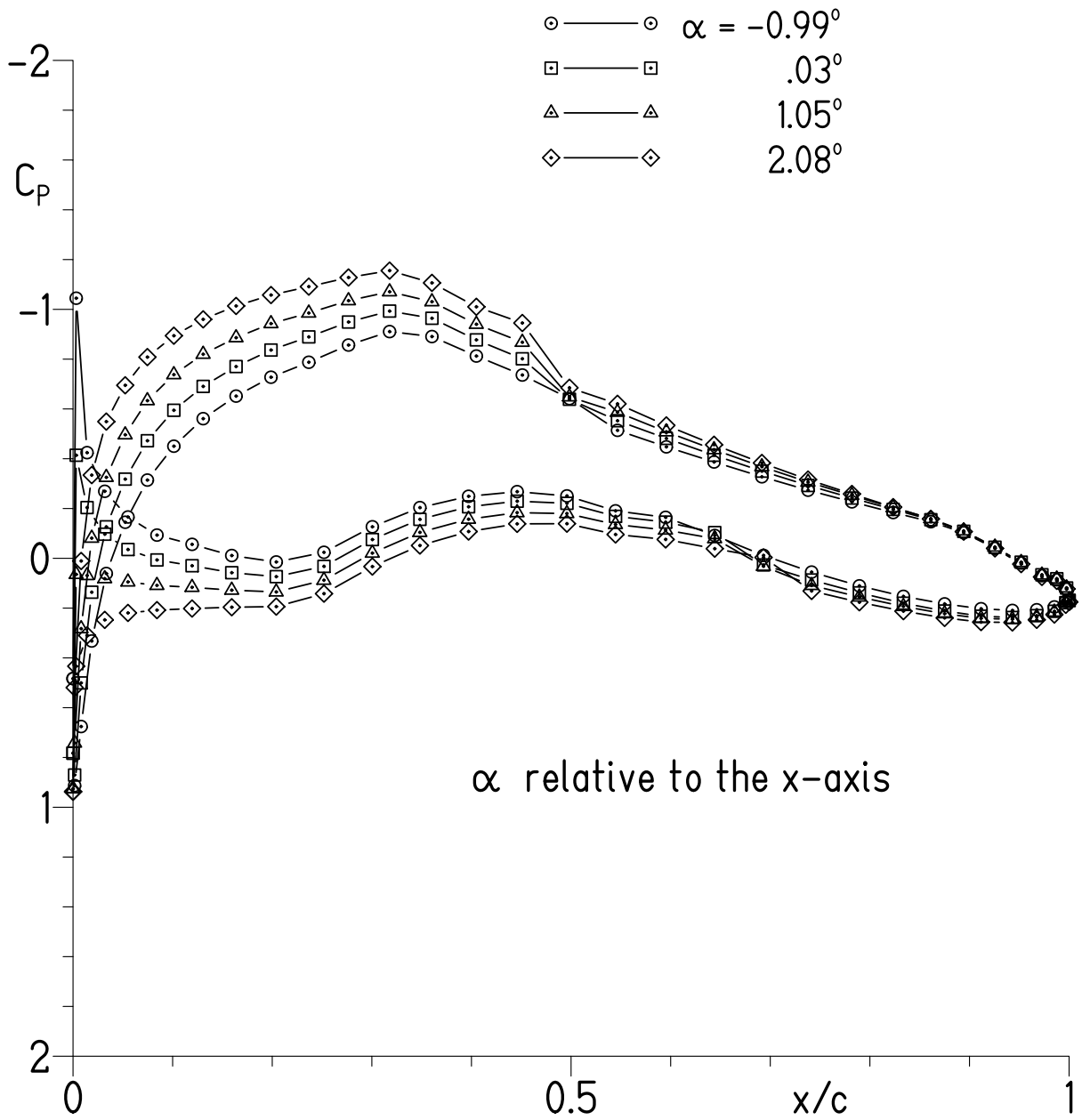
(b) Transition fixed.

Figure 5.- Concluded.



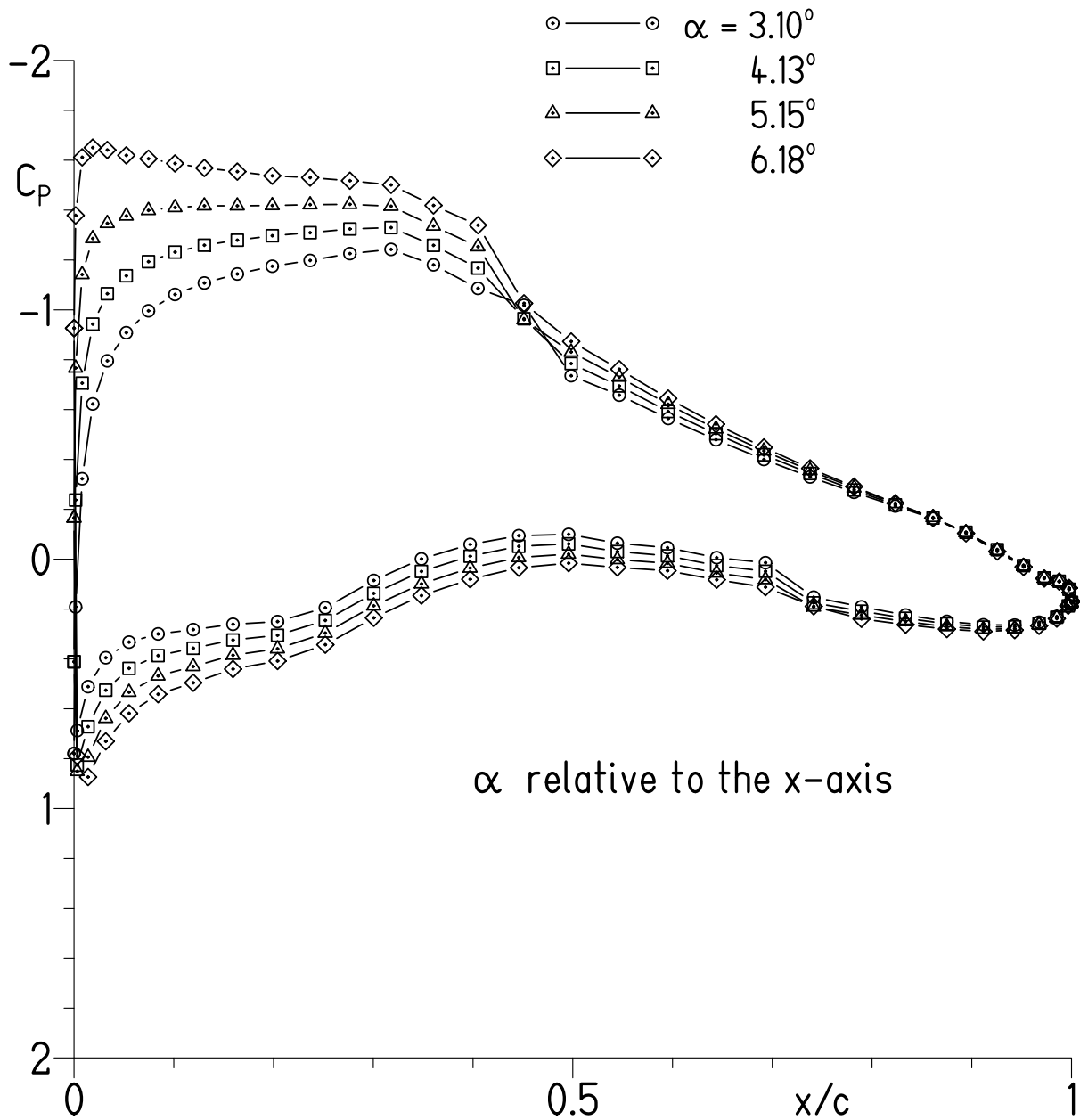
(a) $\alpha = -5.10^\circ, -4.08^\circ, -3.05^\circ,$ and -2.02° .

Figure 6.- Experimental pressure distributions for $R = 1.5 \times 10^6$ and $M = 0.1$ with transition free.



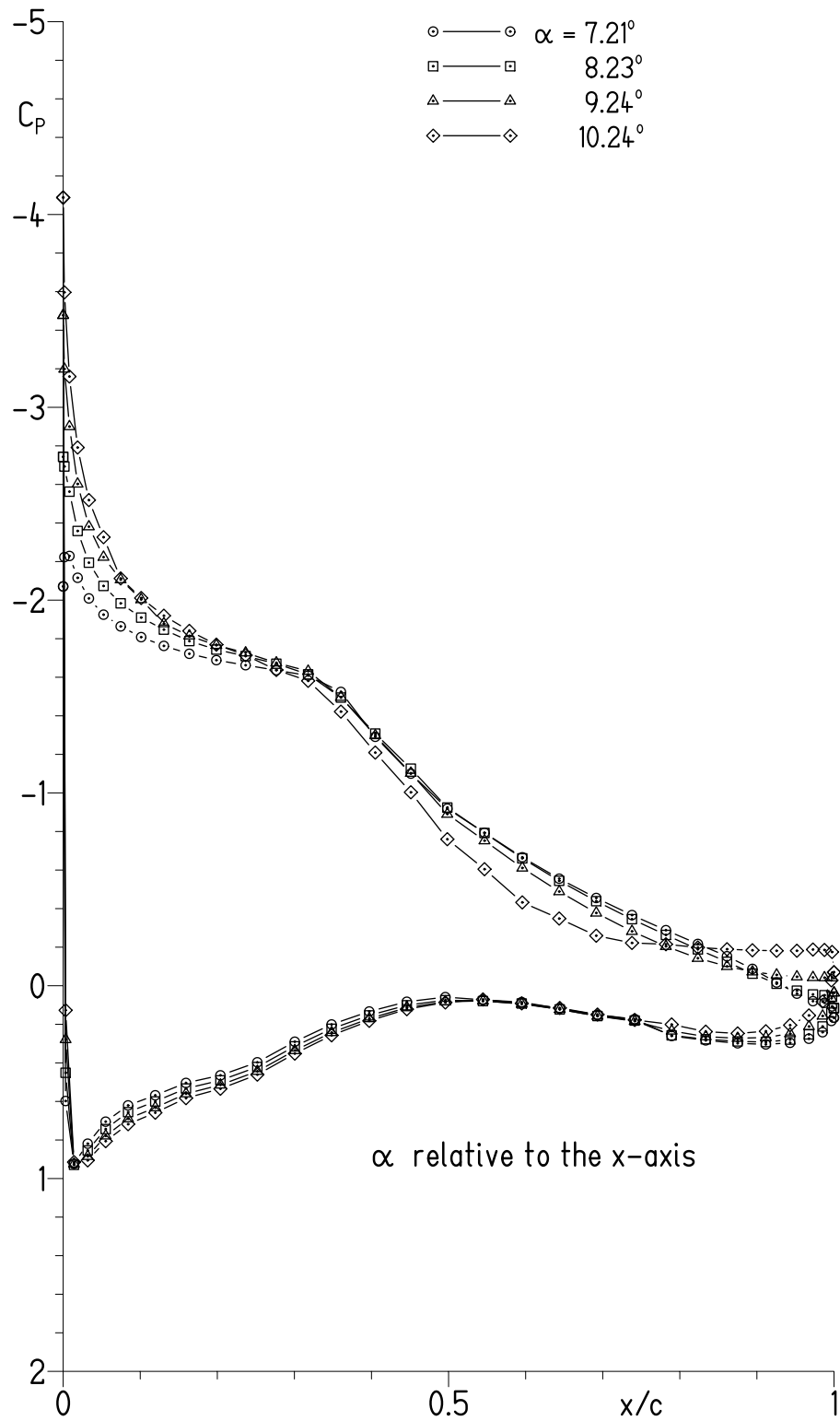
(b) $\alpha = -0.99^\circ, 0.03^\circ, 1.05^\circ,$ and 2.08° .

Figure 6.- Continued.



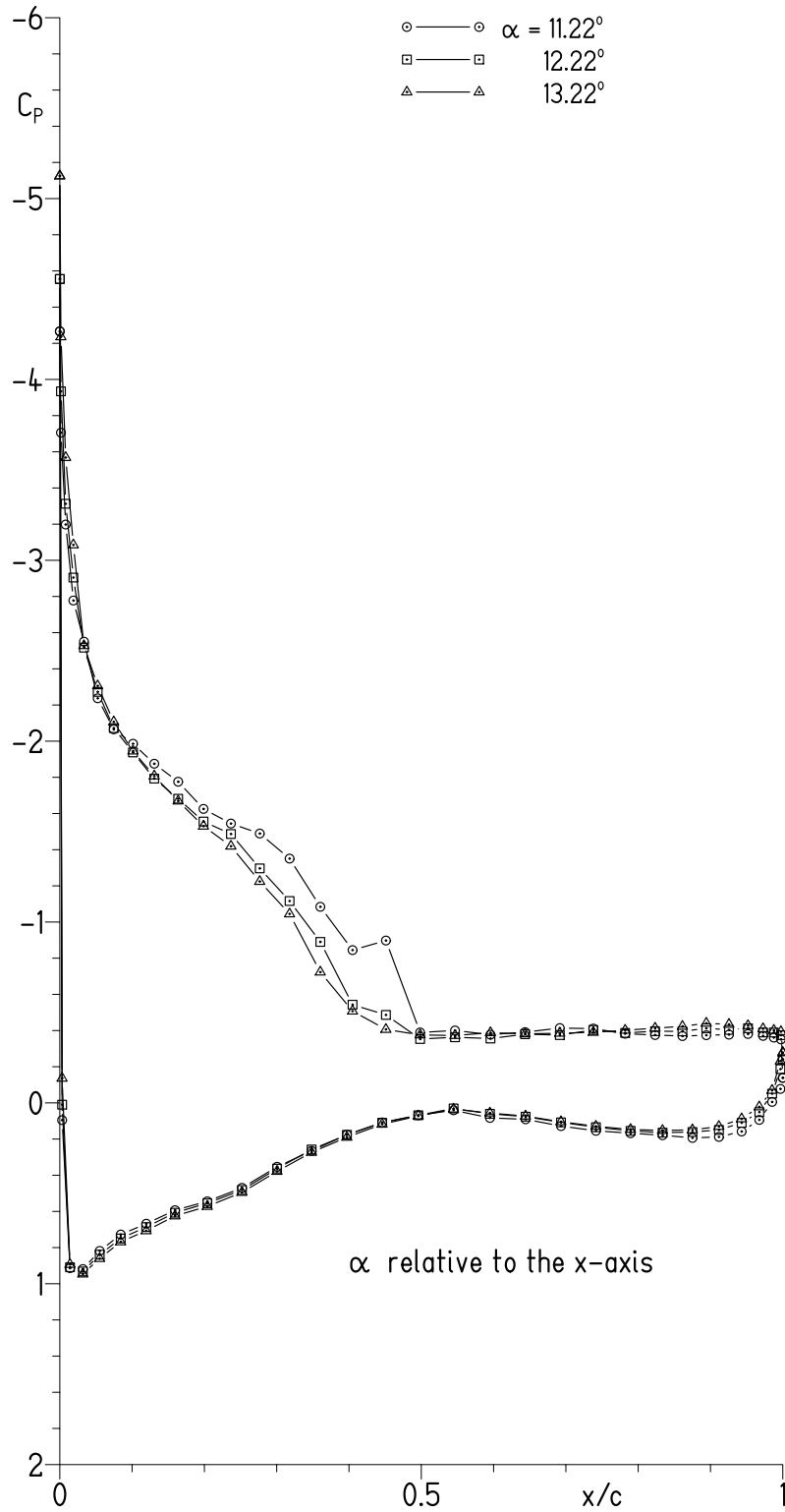
(c) $\alpha = 3.10^\circ, 4.13^\circ, 5.15^\circ, \text{ and } 6.18^\circ$.

Figure 6.- Continued.



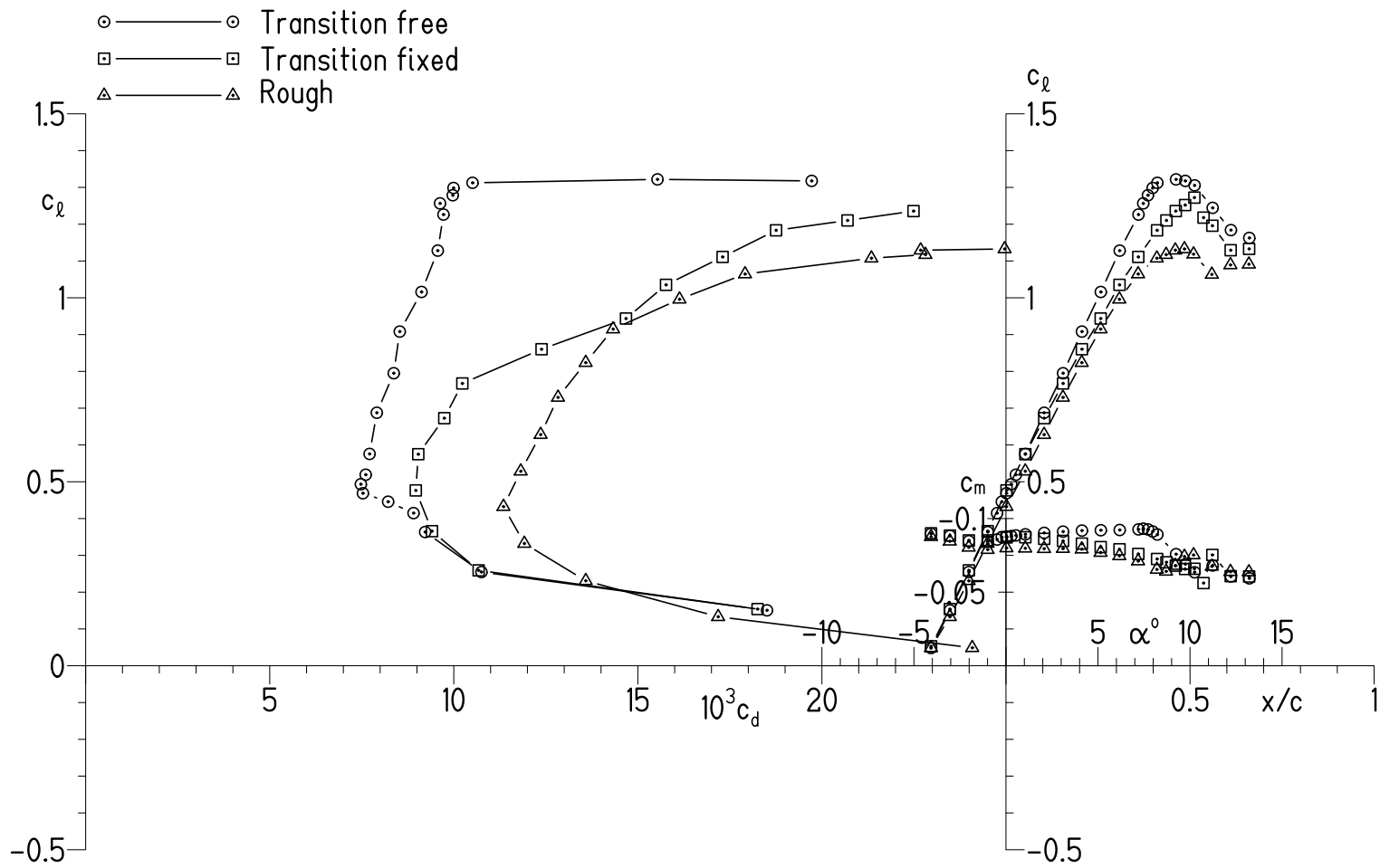
(d) $\alpha = 7.21^\circ, 8.23^\circ, 9.24^\circ,$ and 10.24° .

Figure 6.- Continued.



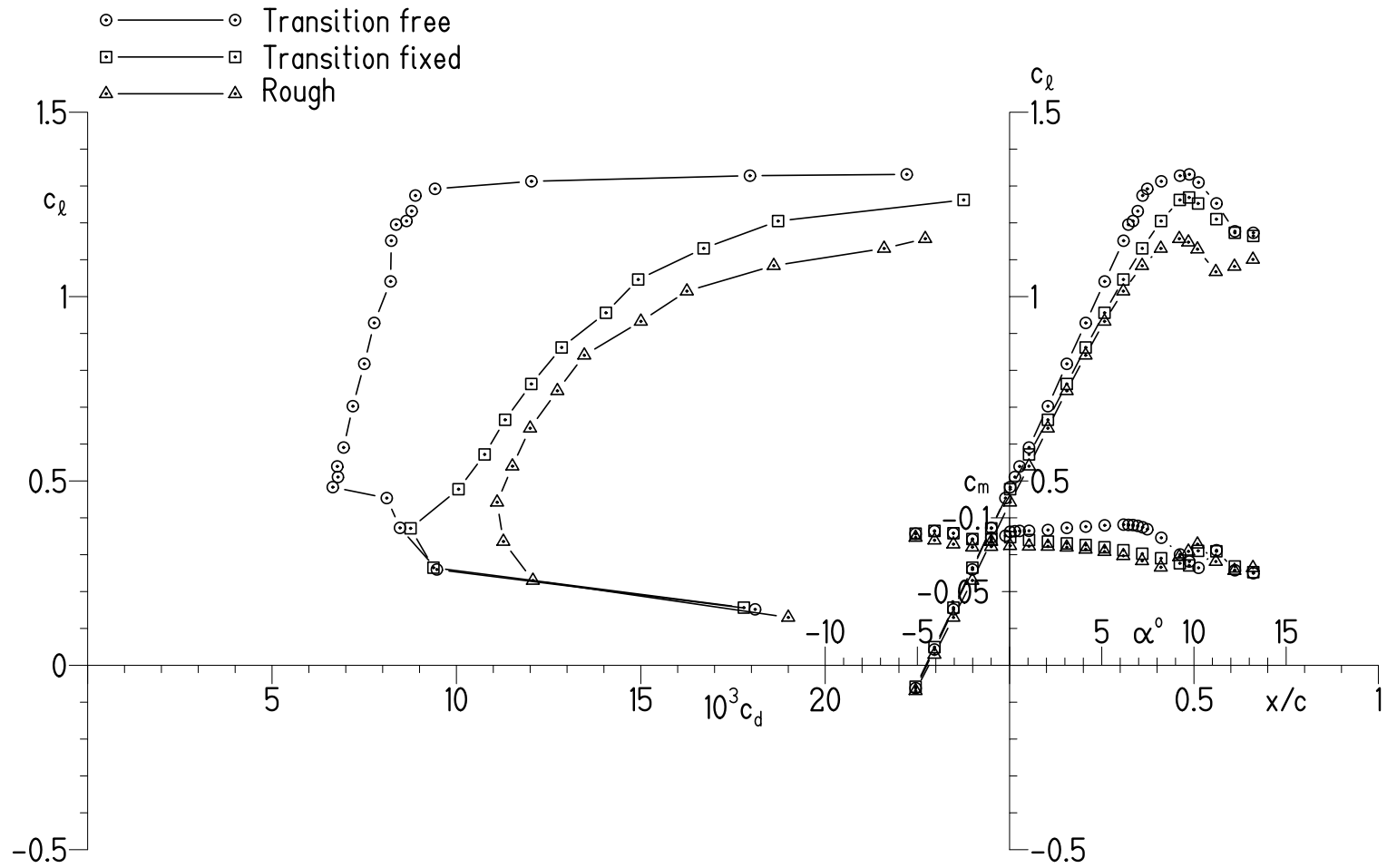
(e) $\alpha = 11.22^\circ, 12.22^\circ, \text{ and } 13.22^\circ$.

Figure 6.- Concluded.



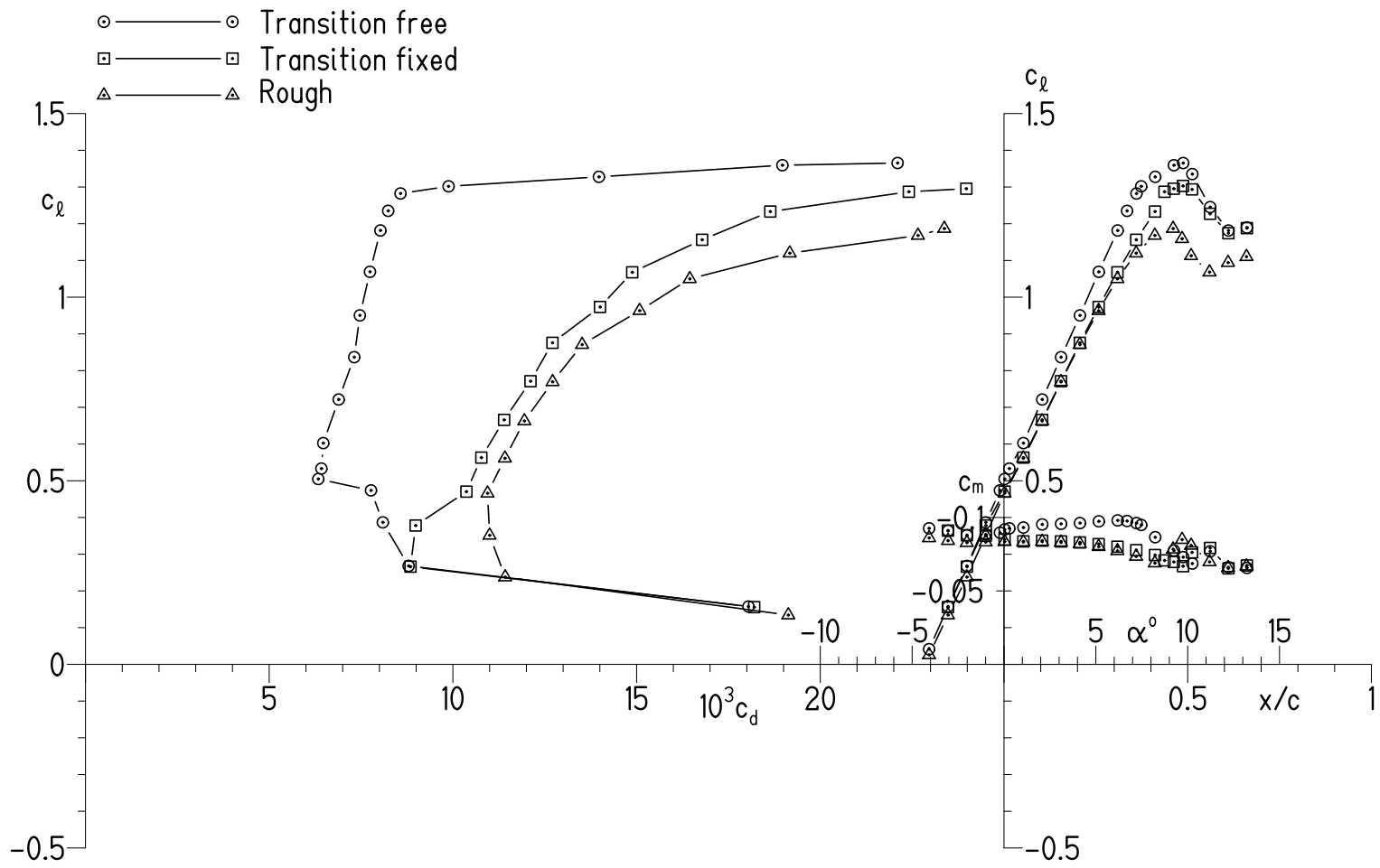
(a) $R = 1.0 \times 10^6$ and $M = 0.1$.

Figure 7.- Experimental section characteristics with transition free, with transition fixed, and rough.



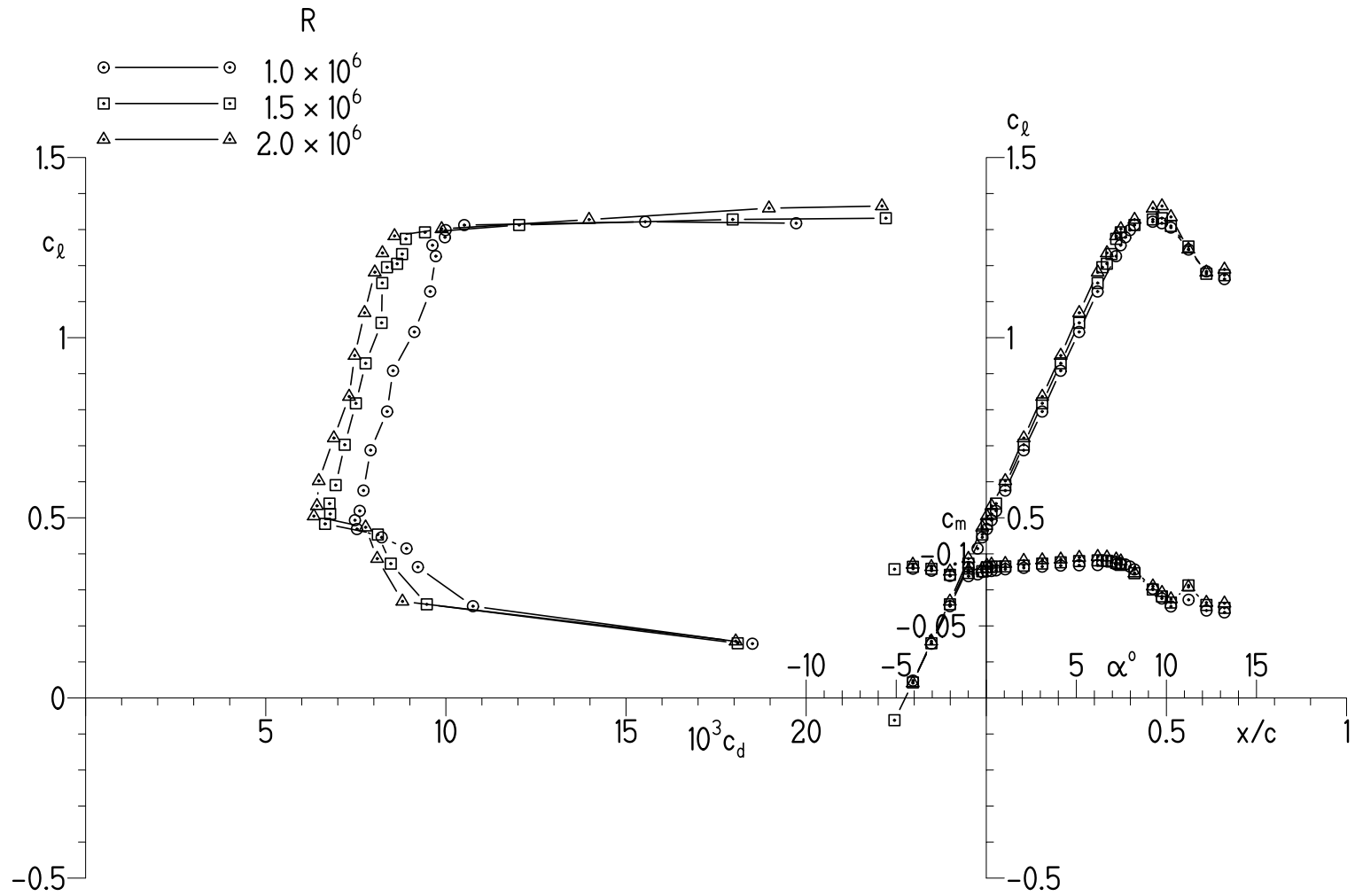
(b) $R = 1.5 \times 10^6$ and $M = 0.1$.

Figure 7.- Continued.



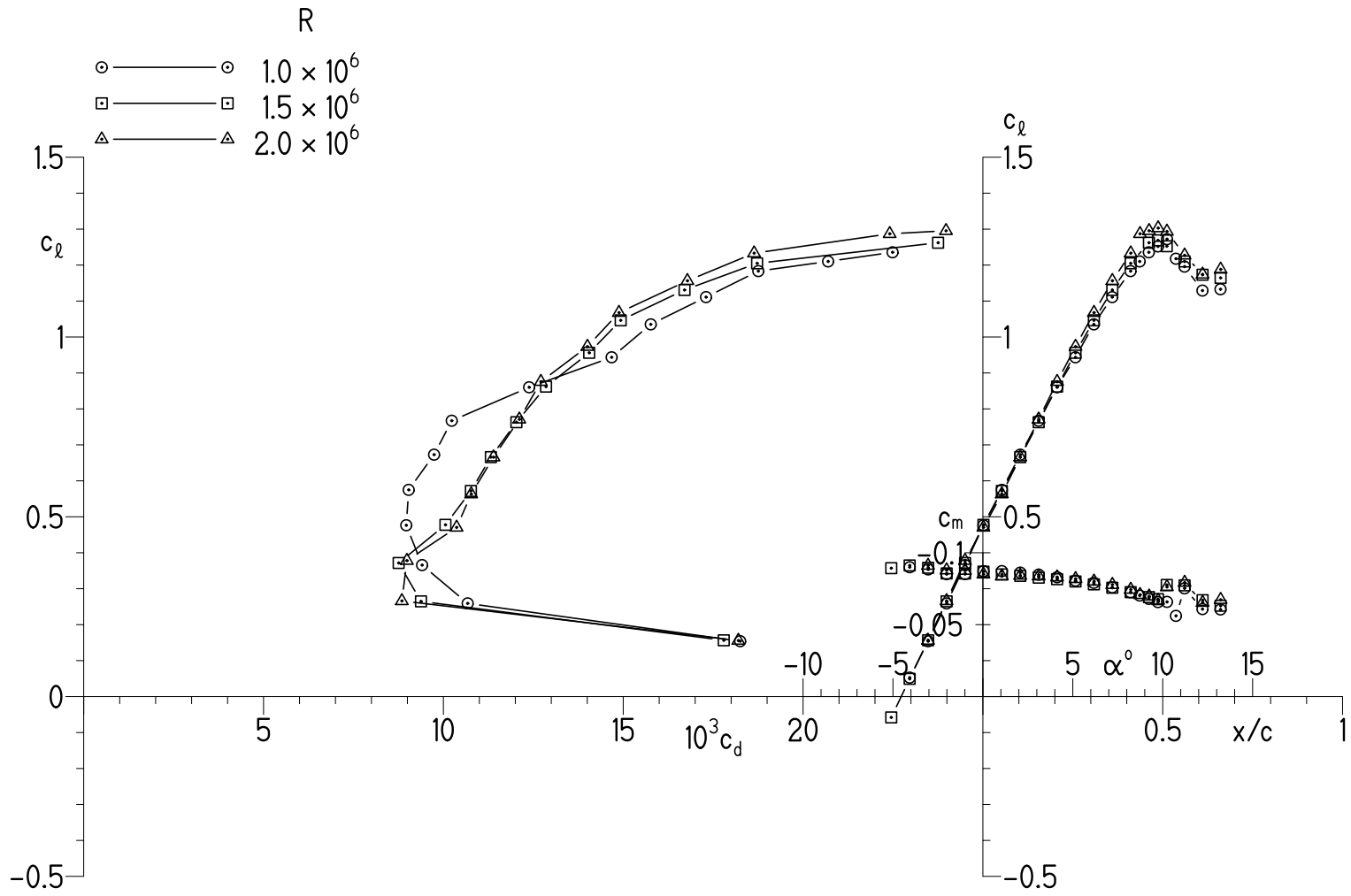
(c) $R = 2.0 \times 10^6$ and $M = 0.2$.

Figure 7.- Concluded.



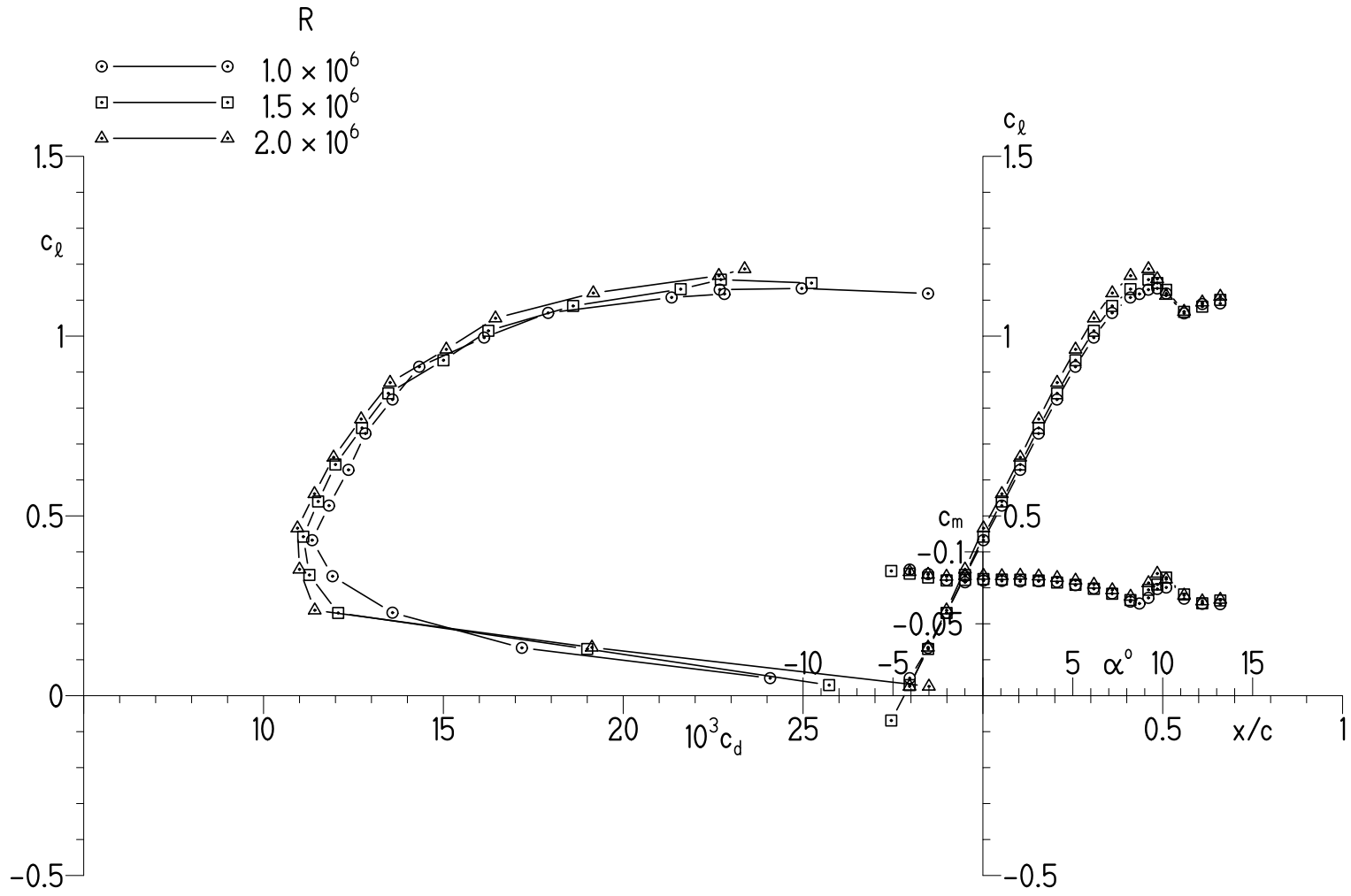
(a) Transition free.

Figure 8.- Effects of Reynolds number on experimental section characteristics.



(b) Transition fixed.

Figure 8.- Continued.



(c) Rough.

Figure 8.- Concluded.

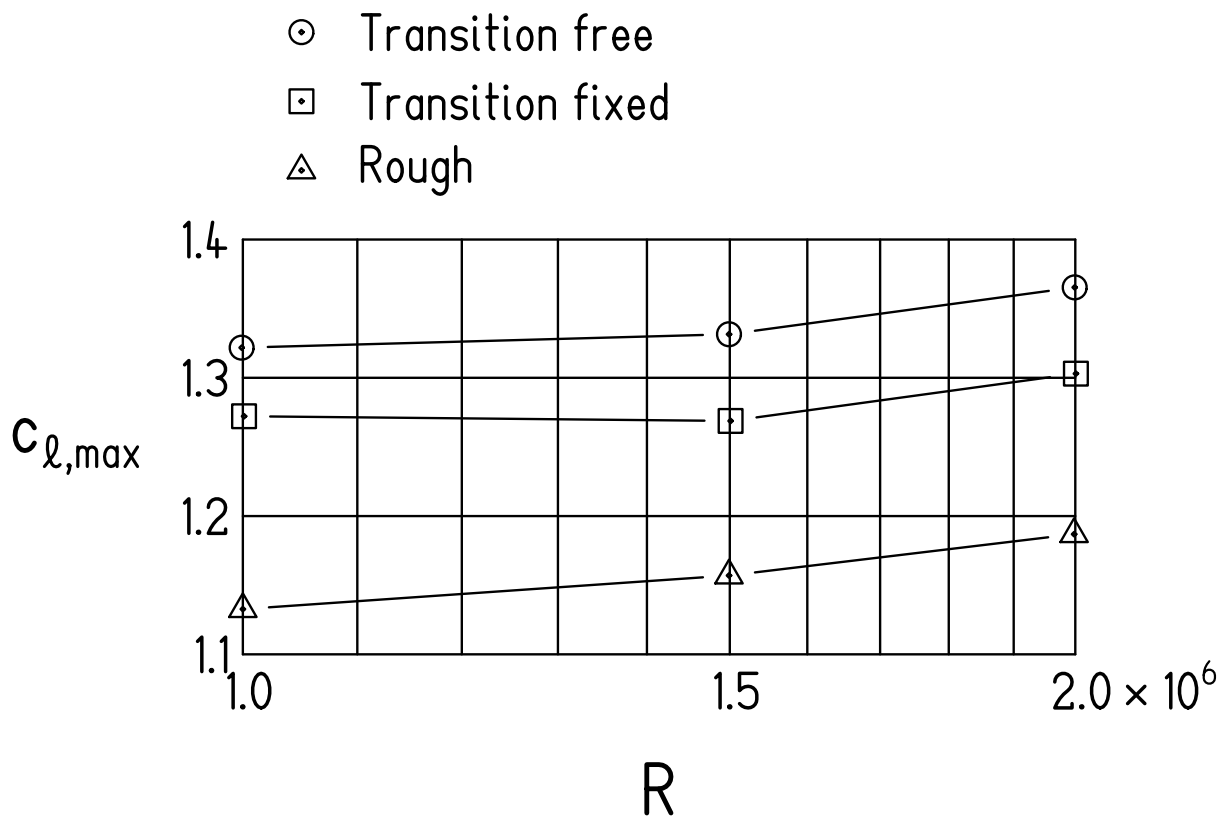


Figure 9.- Variation of experimental maximum lift coefficient with Reynolds number.

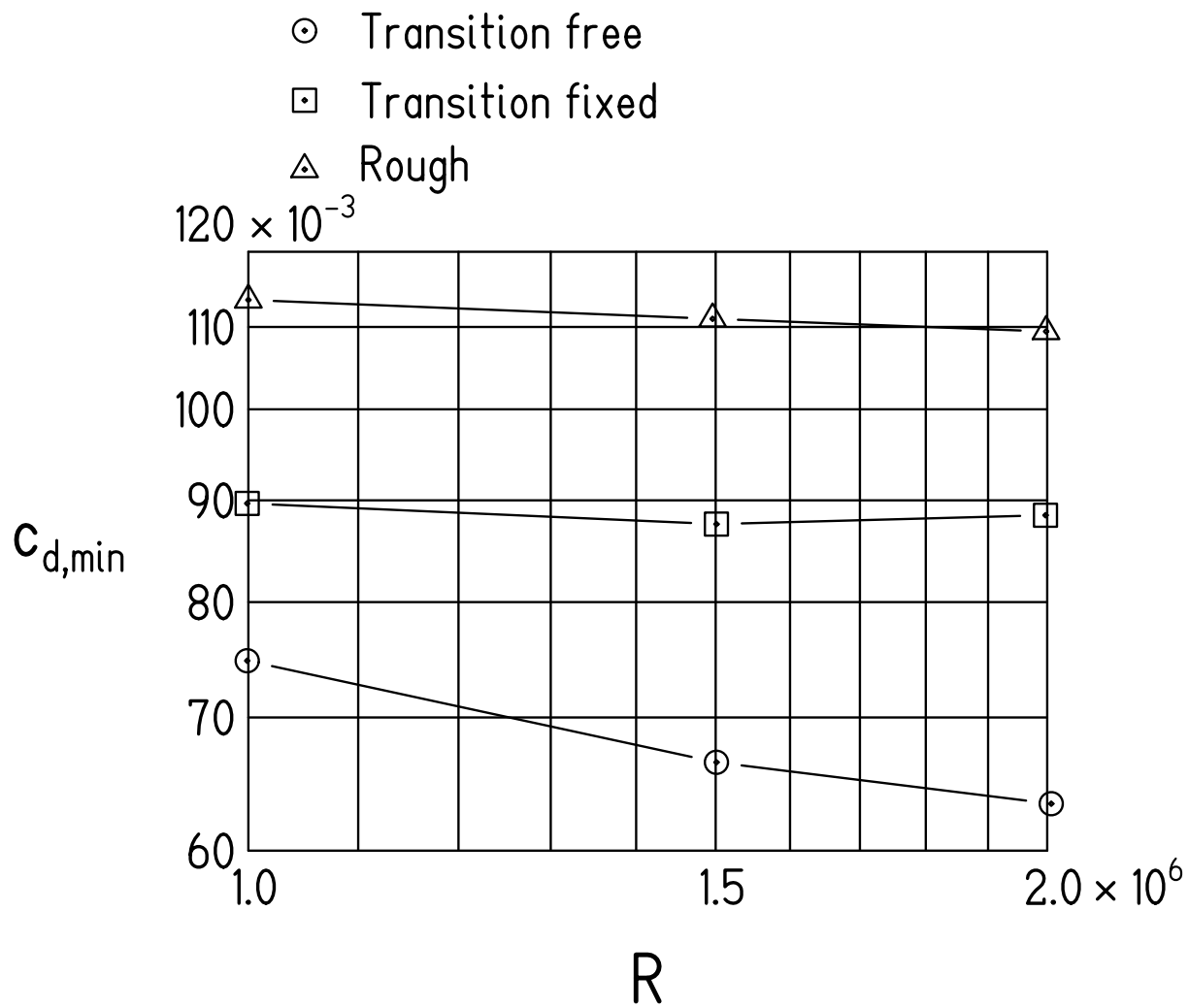
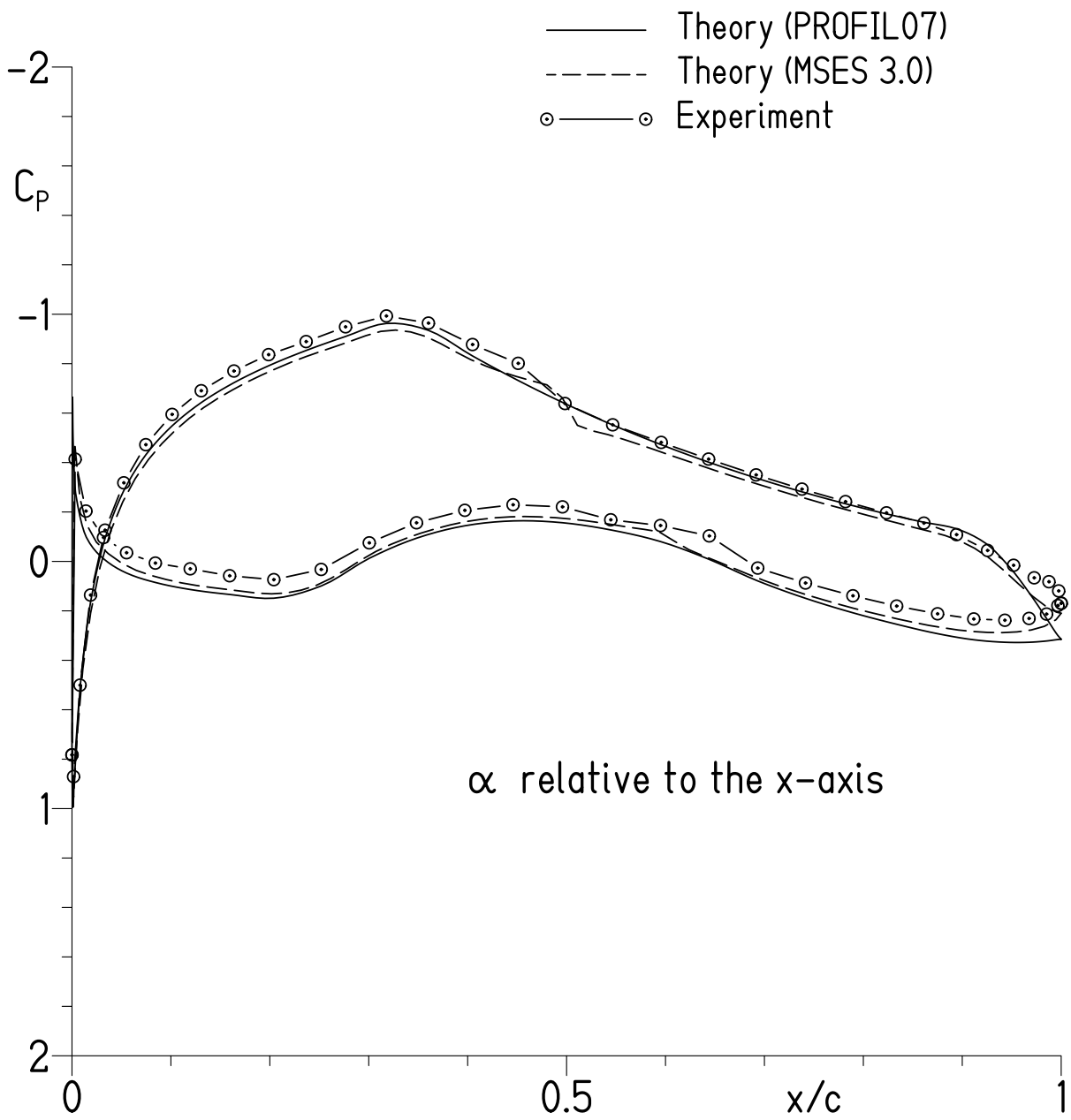
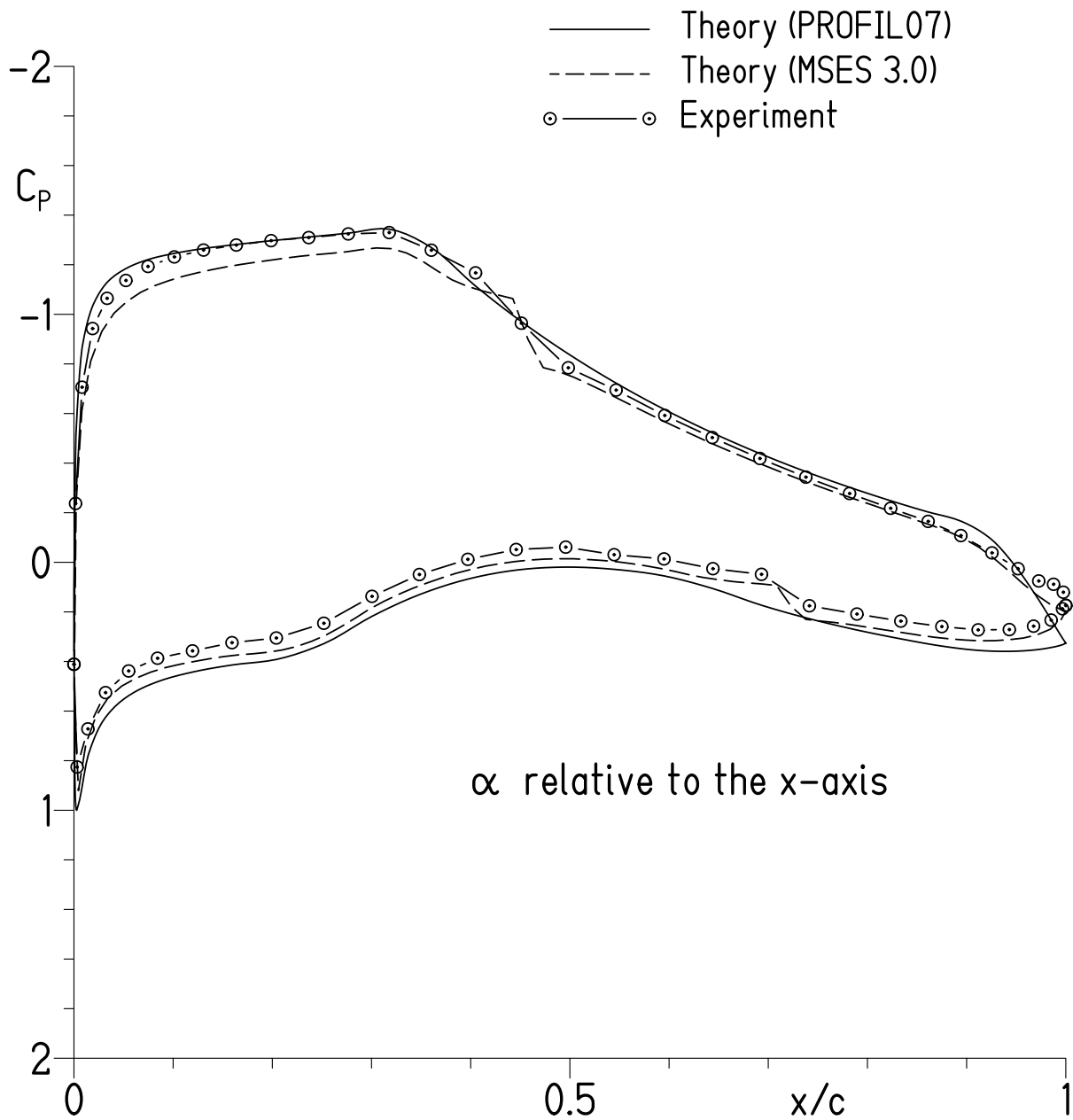


Figure 10.- Variation of experimental minimum profile-drag coefficient with Reynolds number.



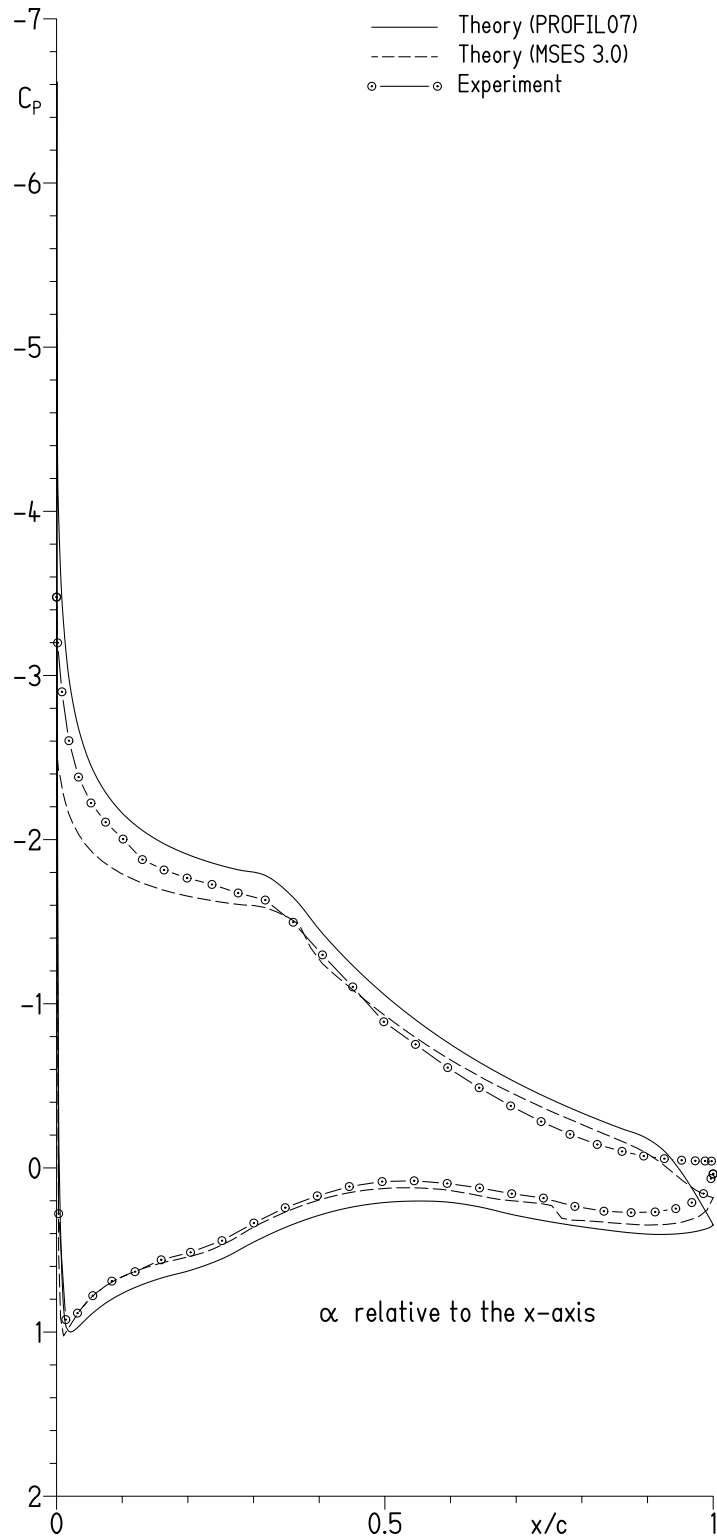
(a) $c_l = 0.48$.

Figure 11.- Comparison of theoretical and experimental pressure distributions for $R = 1.5 \times 10^6$ and $M = 0.1$ with transition free.



(b) $c_l = 0.93$.

Figure 11.- Continued.



(c) $c_l = 1.33$.

Figure 11.- Concluded.

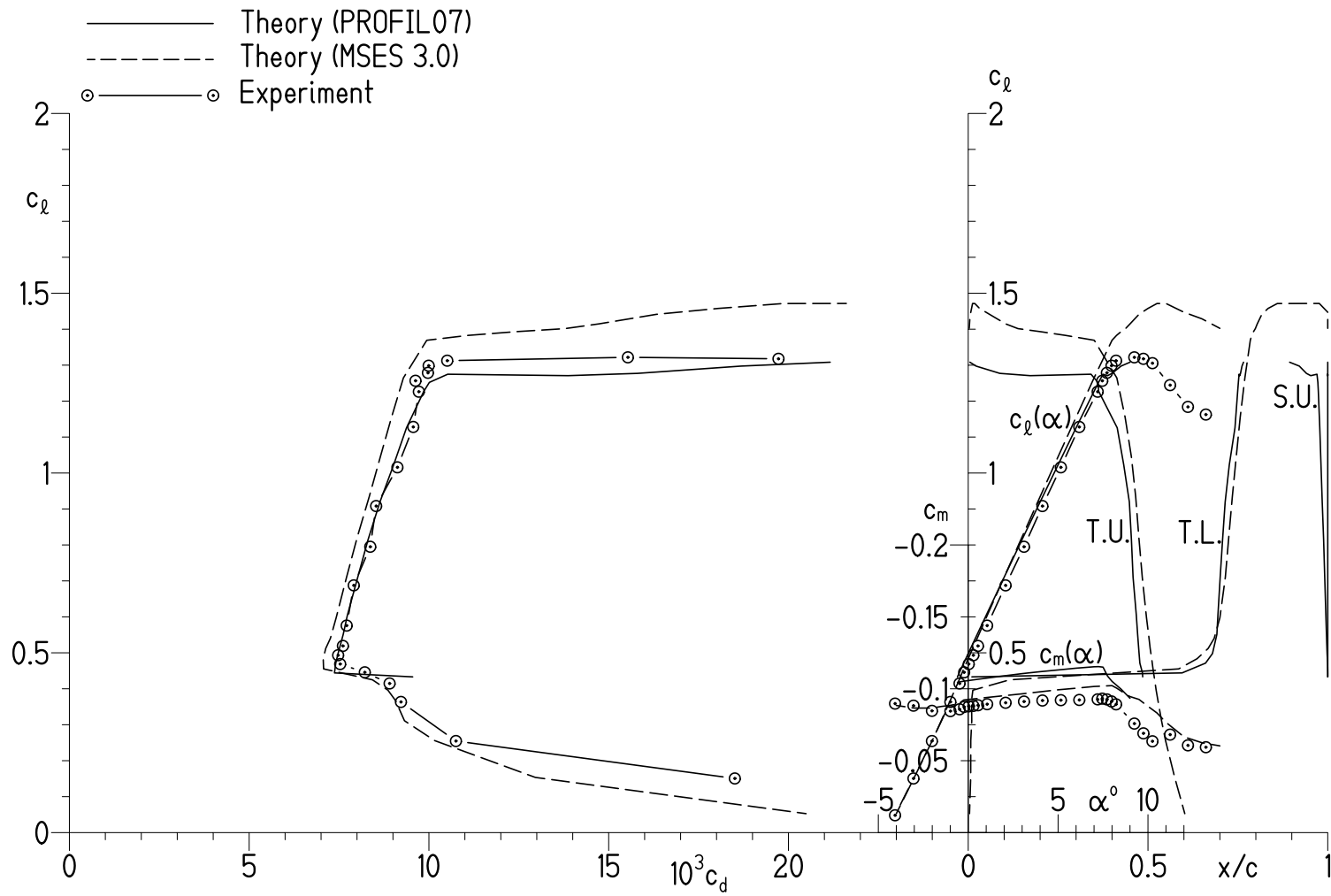
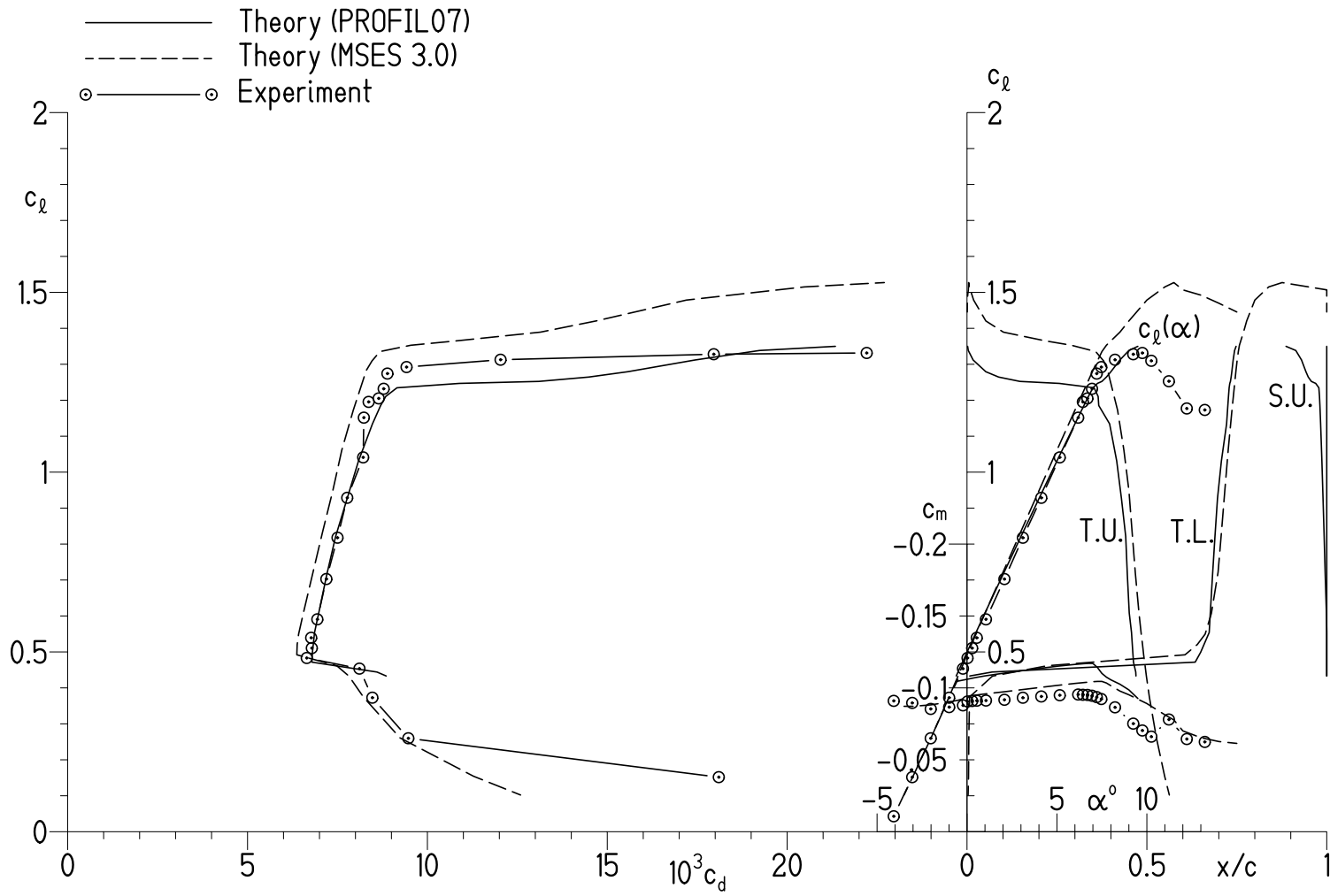
(a) $R = 1.0 \times 10^6$ and $M = 0.1$.

Figure 12.- Comparison of theoretical and experimental section characteristics with transition free.



(b) $R = 1.5 \times 10^6$ and $M = 0.1$.

Figure 12.- Continued.

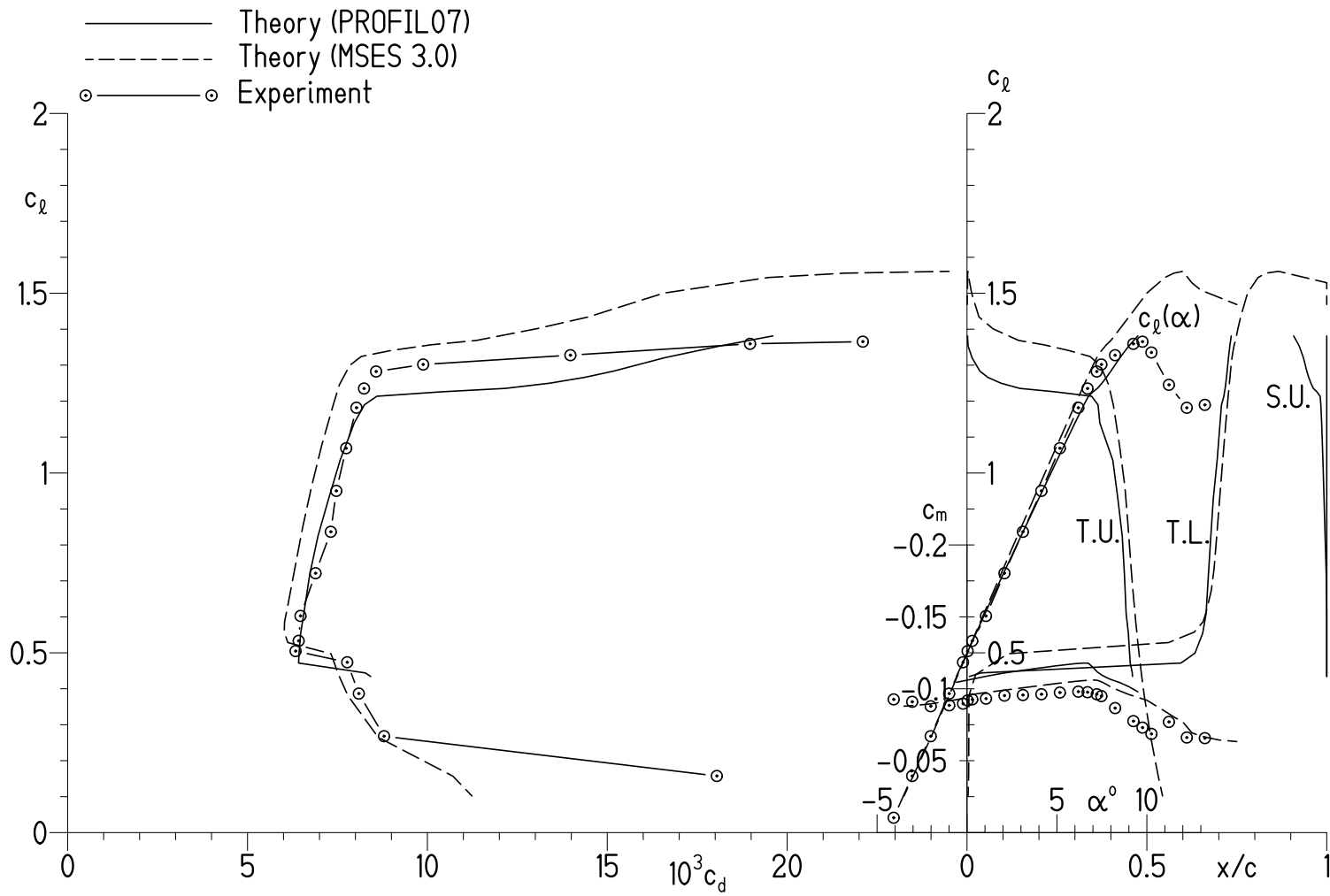
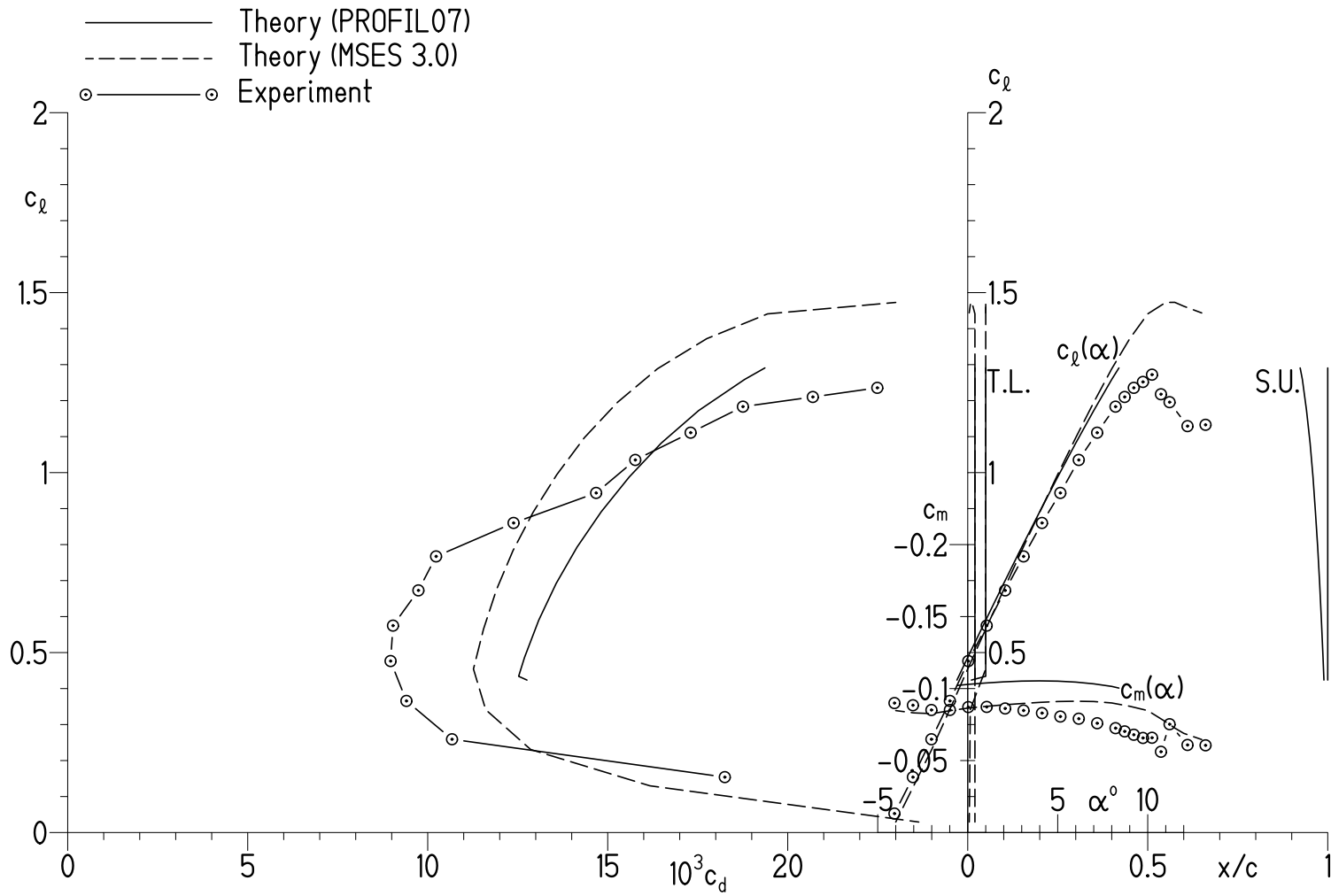
(c) $R = 2.0 \times 10^6$ and $M = 0.2$.

Figure 12.- Concluded.



(a) $R = 1.0 \times 10^6$ and $M = 0.1$.

Figure 13.- Comparison of theoretical and experimental section characteristics with transition fixed.

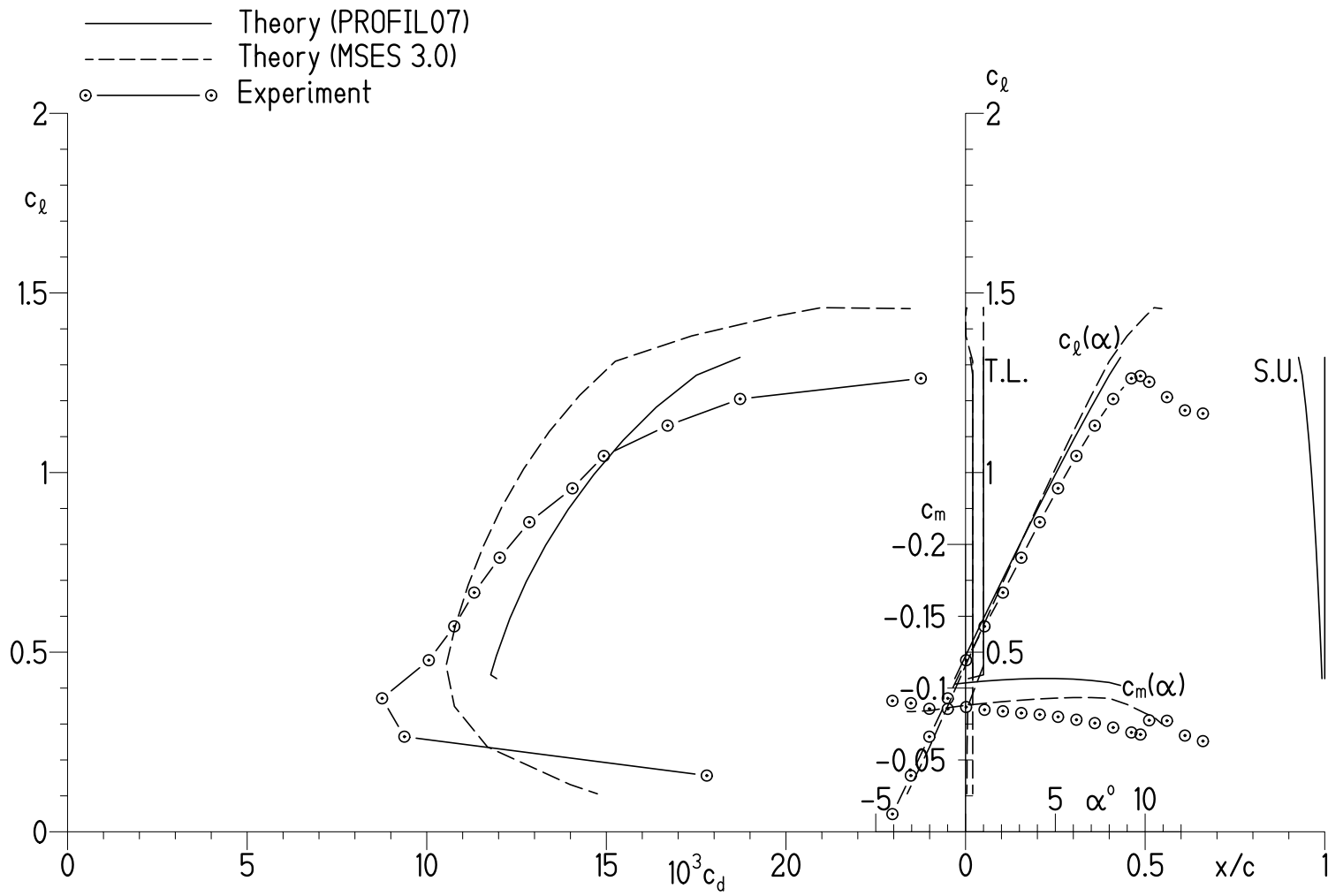
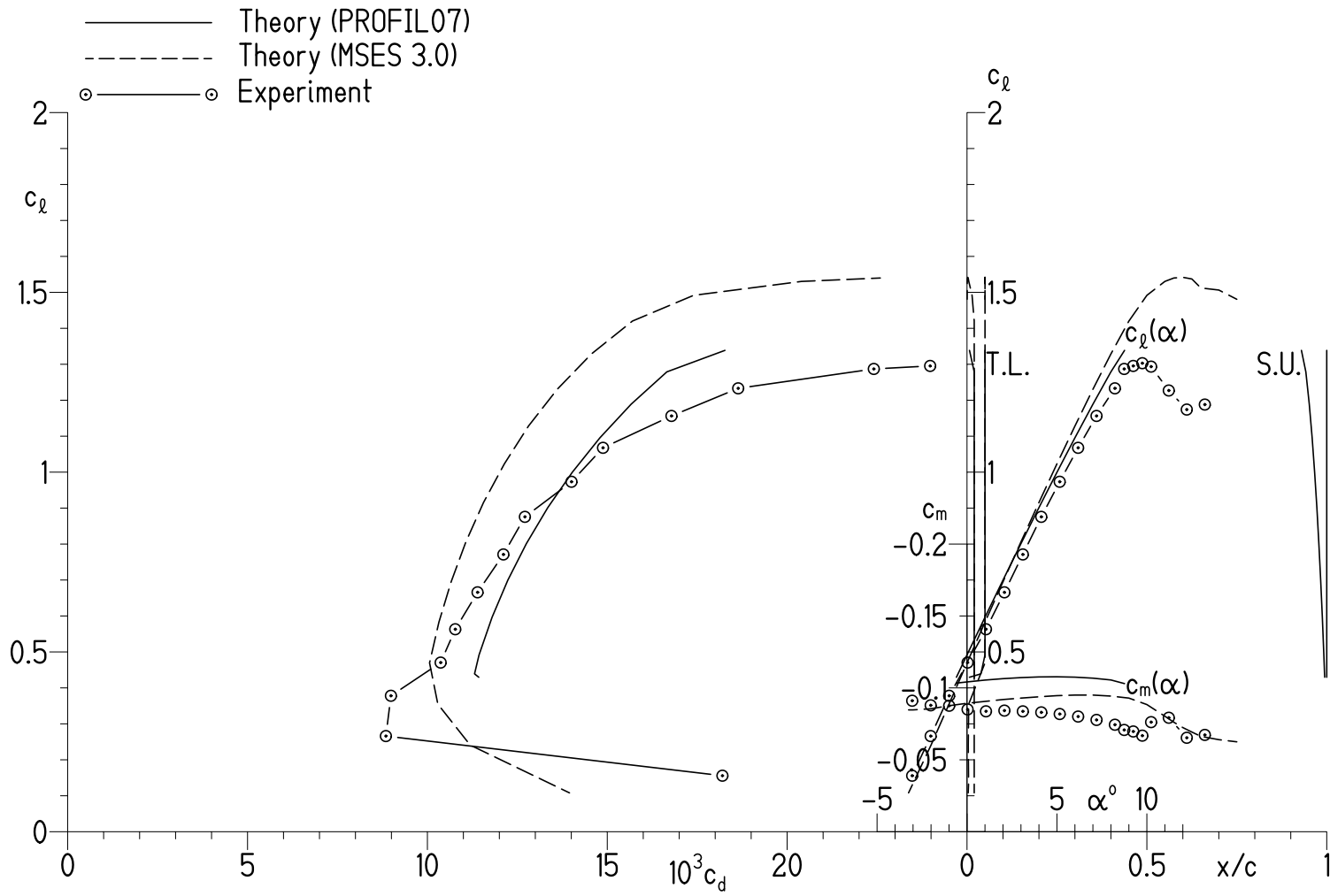
(b) $R = 1.5 \times 10^6$ and $M = 0.1$.

Figure 13.- Continued.



(c) $R = 2.0 \times 10^6$ and $M = 0.2$.

Figure 13.- Concluded.

APPENDIX

EXPERIMENTAL SECTION CHARACTERISTICS

$R = 1.00 \times 10^6$, $M = 0.08$, transition free

α , deg	c_l	c_d	c_m
-4.072	0.0482	0.026784	-0.08971
-3.047	.1506	.018508	-.08828
-2.020	.2547	.010751	-.08468
-.994	.3634	.009222	-.08450
-.484	.4148	.008906	-.08577
-.228	.4458	.008216	-.08743
.027	.4688	.007531	-.08783
.282	.4933	.007475	-.08812
.538	.5192	.007607	-.08855
1.050	.5757	.007712	-.08930
2.076	.6876	.007909	-.09030
3.100	.7950	.008368	-.09114
4.125	.9082	.008532	-.09186
5.150	1.0159	.009123	-.09210
6.176	1.1282	.009564	-.09225
7.199	1.2262	.009719	-.09266
7.455	1.2566	.009626	-.09317
7.711	1.2787	.009972	-.09263
7.967	1.2985	.009992	-.09123
8.222	1.3125	.010509	-.08920
9.237	1.3218	.015533	-.07582
9.742	1.3177	.019722	-.06904
1.245	1.3056	.025156	-.06352
11.227	1.2445	.035996	-.06816
12.220	1.1840	.043106	-.06069
13.217	1.1627	.055247	-.05940

$R = 1.00 \times 10^6$, $M = 0.08$, transition fixed

α , deg	c_l	c_d	c_m
-4.072	0.0528	0.026468	-0.08995
-3.047	.1540	.018252	-.08843
-2.019	.2592	.010675	-.08513
-.994	.3657	.009408	-.08518
.029	.4765	.008968	-.08716
1.052	.5749	.009035	-.08727
2.076	.6728	.009741	-.08620
3.099	.7672	.010232	-.08479
4.123	.8602	.012384	-.08298
5.144	.9436	.014678	-.08059
6.167	1.0352	.015765	-.07911
7.188	1.1110	.017302	-.07595
8.208	1.1833	.018755	-.07252
8.716	1.2102	.020696	-.07027
9.224	1.2356	.022488	-.06796
9.731	1.2520	.026197	-.06572
1.235	1.2722	.023339	-.06586
1.732	1.2178	.109652	-.05614
11.210	1.1958	.126229	-.07527
12.207	1.1292	.159061	-.06086
13.209	1.1329	.191461	-.06061

$R = 1.00 \times 10^6$, $M = 0.08$, rough

α , deg	c_l	c_d	c_m
-4.070	0.0488	0.024084	-0.08768
-3.048	.1331	.017182	-.08460
-2.021	.2309	.013585	-.08046
-.996	.3322	.011917	-.07890
.026	.4325	.011350	-.08000
1.049	.5287	.011819	-.07981
2.072	.6281	.012360	-.07952
3.095	.7292	.012832	-.07961
4.118	.8238	.013584	-.07920
5.141	.9149	.014328	-.07691
6.162	.9960	.016132	-.07464
7.181	1.0646	.017912	-.07113
8.197	1.1075	.021345	-.06542
8.701	1.1173	.022813	-.06412
9.200	1.1293	.022682	-.06805
9.695	1.1327	.024964	-.07420
1.191	1.1186	.028474	-.07525
11.186	1.0635	.050962	-.06749
12.196	1.0893	.059921	-.06389
13.197	1.0911	.072355	-.06367

$R = 1.50 \times 10^6$, $M = 0.12$, transition free

α , deg	c_l	c_d	c_m
-5.098	-0.0618	0.037471	-0.08927
-4.075	.0430	.027653	-.09100
-3.048	.1518	.018100	-.08958
-2.019	.2599	.009470	-.08540
-.994	.3728	.008470	-.08667
-.226	.4536	.008111	-.08788
.028	.4832	.006646	-.09059
.284	.5107	.006787	-.09093
.540	.5394	.006769	-.09115
1.052	.5907	.006940	-.09124
2.078	.7028	.007191	-.09177
3.103	.8177	.007501	-.09320
4.129	.9287	.007771	-.09407
5.154	1.0411	.008214	-.09494
6.179	1.1516	.008233	-.09543
6.440	1.1954	.008366	-.09524
6.692	1.2051	.008646	-.09514
6.949	1.2319	.008784	-.09459
7.210	1.2742	.008888	-.09363
7.465	1.2923	.009420	-.09229
8.226	1.3127	.012033	-.08652
9.240	1.3280	.017959	-.07519
9.746	1.3315	.022211	-.07042
1.245	1.3098	.041694	-.06615
11.221	1.2529	.041132	-.07806
12.216	1.1772	.043370	-.06449
13.217	1.1731	.054974	-.06248

$R = 1.50 \times 10^6$, $M = 0.13$, transition fixed

α , deg	c_l	c_d	c_m
-5.097	-0.0580	0.037115	-0.08926
-4.074	.0493	.027177	-.09114
-3.047	.1565	.017795	-.08953
-2.018	.2648	.009377	-.08562
-.993	.3715	.008756	-.08554
.030	.4776	.010057	-.08684
1.054	.5719	.010765	-.08492
2.077	.6659	.011320	-.08391
3.101	.7630	.012030	-.08266
4.125	.8620	.012854	-.08159
5.148	.9561	.014054	-.08001
6.171	1.0463	.014929	-.07800
7.194	1.1308	.016704	-.07564
8.214	1.2049	.018722	-.07257
9.231	1.2621	.023754	-.06914
9.734	1.2688	.038114	-.06771
1.221	1.2524	.029319	-.07760
11.212	1.2100	.044823	-.07730
12.213	1.1731	.047744	-.06700
13.215	1.1644	.056824	-.06313

$R = 1.50 \times 10^6$, $M = 0.13$, rough

α , deg	c_l	c_d	c_m
-5.097	-0.0690	0.035415	-0.08669
-4.073	.0295	.025725	-.08484
-3.047	.1299	.018999	-.08215
-2.021	.2301	.012075	-.08009
-.997	.3358	.011274	-.08050
.027	.4422	.011104	-.08109
1.051	.5401	.011518	-.08073
2.075	.6429	.011999	-.08065
3.099	.7445	.012738	-.08005
4.123	.8409	.013468	-.07865
5.146	.9328	.015002	-.07709
6.168	1.0148	.016250	-.07428
7.187	1.0839	.018606	-.07086
8.202	1.1306	.021597	-.06648
9.202	1.1570	.022713	-.07360
9.697	1.1476	.025234	-.07727
1.188	1.1287	.047662	-.08210
11.185	1.0675	.050181	-.07038
12.195	1.0819	.056831	-.06423
13.198	1.1008	.071990	-.06618

$R = 2.00 \times 10^6$, $M = 0.17$, transition free

α , deg	c_l	c_d	c_m
-4.078	0.0414	0.028329	-0.09266
-3.049	.1575	.018045	-.09098
-2.020	.2681	.008795	-.08789
-.993	.3867	.008093	-.08852
-.223	.4738	.007771	-.08969
.032	.5048	.006335	-.09189
.288	.5333	.006421	-.09266
1.054	.6026	.006472	-.09319
2.080	.7214	.006890	-.09530
3.106	.8366	.007314	-.09570
4.133	.9504	.007468	-.09624
5.159	1.0691	.007743	-.09742
6.185	1.1817	.008027	-.09805
6.698	1.2351	.008238	-.09765
7.211	1.2824	.008574	-.09623
7.467	1.3019	.009882	-.09494
8.231	1.3278	.013974	-.08660
9.247	1.3594	.018968	-.07755
9.753	1.3654	.022104	-.07305
1.250	1.3353	.031283	-.06867
11.222	1.2454	.038509	-.07700
12.217	1.1816	.044925	-.06617
13.220	1.1897	.057890	-.06571

$R = 1.99 \times 10^6$, $M = 0.17$, transition fixed

α , deg	c_l	c_d	c_m
-3.049	0.1558	0.018201	-0.09108
-2.020	.2660	.008846	-.08789
-.994	.3781	.008986	-.08760
.030	.4704	.010368	-.08504
1.053	.5631	.010774	-.08372
2.077	.6658	.011394	-.08422
3.102	.7711	.012112	-.08369
4.128	.8757	.012710	-.08299
5.152	.9733	.014005	-.08185
6.176	1.0677	.014881	-.08009
7.199	1.1563	.016784	-.07775
8.220	1.2331	.018639	-.07441
8.737	1.2870	.022409	-.07077
9.240	1.2954	.023975	-.06971
9.744	1.3030	.027872	-.06682
1.233	1.2935	.030545	-.07621
11.216	1.2271	.045895	-.07927
12.216	1.1741	.046306	-.06534
13.219	1.1880	.062936	-.06733

$R = 2.00 \times 10^6$, $M = 0.18$, rough

α , deg	c_l	c_d	c_m
-4.075	0.0258	0.028500	-0.08610
-3.048	.1343	.019130	-.08422
-2.022	.2377	.011424	-.08288
-.996	.3514	.010999	-.08322
.031	.4659	.010943	-.08353
1.054	.5613	.011416	-.08325
2.077	.6628	.011947	-.08357
3.103	.7694	.012714	-.08306
4.128	.8708	.013518	-.08201
5.151	.9632	.015081	-.08013
6.175	1.0499	.016448	-.07730
7.195	1.1198	.019168	-.07348
8.211	1.1681	.022659	-.06895
9.206	1.1869	.023375	-.07838
9.695	1.1591	.038048	-.08493
1.187	1.1127	.047673	-.08097
11.188	1.0682	.051510	-.06974
12.198	1.0942	.059991	-.06574
13.201	1.1102	.073498	-.06685

REPORT DOCUMENTATION PAGE

Form Approved
OMB No. 0704-0188

Public reporting burden for this collection of information is estimated to average 1 hour per response, including the time for reviewing instructions, searching existing data sources, gathering and maintaining the data needed, and completing and reviewing this collection of information. Send comments regarding this burden estimate or any other aspect of this collection of information, including suggestions for reducing this burden to Department of Defense, Washington Headquarters Services, Directorate for Information Operations and Reports (0704-0188), 1215 Jefferson Davis Highway, Suite 1204, Arlington, VA 22202-4302. Respondents should be aware that notwithstanding any other provision of law, no person shall be subject to any penalty for failing to comply with a collection of information if it does not display a currently valid OMB control number. **PLEASE DO NOT RETURN YOUR FORM TO THE ABOVE ADDRESS.**

1. REPORT DATE (DD-MM-YYYY) xx 08 2010	2. REPORT TYPE FINAL REPORT	3. DATES COVERED (From - To) Sep 2007 Jun 2010
--	---------------------------------------	--

4. TITLE AND SUBTITLE Design and Experimental Results for the S415 Airfoil	5a. CONTRACT NUMBER W911W6 07 C 0047
	5b. GRANT NUMBER
	5c. PROGRAM ELEMENT NUMBER

6. AUTHOR(S) Somers, Dan M. and Maughmer, Mark D.	5d. PROJECT NUMBER
	5e. TASK NUMBER
	5f. WORK UNIT NUMBER

7. PERFORMING ORGANIZATION NAME(S) AND ADDRESS(ES) Airfoils, Incorporated Attn: Dan M. Somers 122 Rose Drive Port Matilda PA 16870 7535	8. PERFORMING ORGANIZATION REPORT NUMBER SBIR Topic Number A06 006 Proposal Number A2 2972
--	---

9. SPONSORING / MONITORING AGENCY NAME(S) AND ADDRESS(ES) US Army Aviation Research, Development and Engineering Command (RDECOM) Aviation Applied Technology Directorate (AATD) Fort Eustis VA 23604 5577	10. SPONSOR/MONITOR'S ACRONYM(S)
	11. SPONSOR/MONITOR'S REPORT NUMBER(S) RDECOM TR 10 D 114

12. DISTRIBUTION / AVAILABILITY STATEMENT Approved for public release; distribution is unlimited.

13. SUPPLEMENTARY NOTES UL Note: No proprietary / limited information may be included in the abstract.
--

14. ABSTRACT A 14.12 percent thick, natural laminar flow airfoil, the S415, intended for the rotor of a helicopter in hover has been designed and analyzed theoretically and verified experimentally in The Pennsylvania State University Low Speed, Low Turbulence Wind Tunnel. The two primary objectives of high maximum lift and low profile drag have been achieved. The constraint on the pitching moment has been satisfied. The airfoil exhibits a docile stall. Comparisons of the theoretical and experimental results generally show good agreement.

15. SUBJECT TERMS Airfoils, rotorcraft, laminar flow, wind tunnel

16. SECURITY CLASSIFICATION OF:			17. LIMITATION OF ABSTRACT UU	18. NUMBER OF PAGES 57	19a. NAME OF RESPONSIBLE PERSON Dan M. Somers
a. REPORT unclassified	b. ABSTRACT unclassified	c. THIS PAGE unclassified			19b. TELEPHONE NUMBER (include area code) (814) 357 0500